universität wien

MASTERARBEIT / MASTER'S THESIS

Titel der Masterarbeit / Title of the Master's Thesis

The Arctic Freshwater Budget

verfasst von / submitted by

Susanna Winkelbauer, BSc

angestrebter akademischer Grad / in partial fulfilment of the requirements for the degree of

Master of Science (MSc)

Wien, 2020 / Vienna, 2020

Studienkennzahl lt. Studienblatt / degree programme code as it appears on the student record sheet:	UA 066 614
Studienrichtung lt. Studienblatt: degree programme as it appears on the student record sheet:	Masterstudium Meteorologie
Betreuer / Supervisor:	Univ.-Prof. Mag. Dr. Leopold Haimberger

Contents

Abstract

In this thesis the freshwater budget of the Arctic and all it's relevant components is discussed. Therefore the Arctic system is divided into it's three branches, the atmosphere, the land and the ocean, and budget equations for the subsystems are constructed. The individual hydrological components are then examined, using essentially the newest ECMWF reanalysis ERA5, and, if available, compared to other datasets and previous studies. The parameters are analysed on their spatial distribution, seasonalities, interannual variabilities and possible trends. Several hydrological variables exhibit significant changes over the past decades, e.g. the central Arctic indicates a slight increase of freshwater delivery from the atmosphere to the surface, while peripheral oceanic regions like Kara, Barents and Beaufort Sea show relatively strong decreases.

The biggest inconsistencies were found concerning the hydrological land variable runoff, with values from ERA5 showing strong negative trends over the past decades and hence differing greatly from observed runoff values, that feature rather positive trends. As runoff from ERA5-Land, the offline simulation of ERA5, showed considerably higher values, the problem was attributed mainly to the data assimilation system and the introduction of a new IMS (Interactive Multi-sensor Snow and Ice Mapping System) snow cover product in 2004.

Zusammenfassung

In dieser Arbeit wird der Süßwasserhaushalt der Arktis mit all seinen Komponenten diskutiert. Dazu wird die Arktis in die Zweige Atmosphäre, Land und Ozean aufgeteilt und Haushaltsgleichungen für die drei Subsysteme aufgestellt. Die einzelnen Süßwasserkomponenten werden anschließend untersucht, wobei hauptsächlich das neuste ECMWF Reanalyseprodukt ERA5 verwendet wird. Die Parameter werden untersucht auf Saisonalität, zwischenjährliche Variabilität und Trends. So zeigt beispielsweise die mittlere Arktis einen leichten Zuwachs an Süßwasserzufuhr von der Atmosphäre zur Oberfläche, während Regionen wie die Karasee, Barentssee und Beaufortsee relativ beträchtliche Abnahmen verzeichnen.

Die Größten Unstimmigkeiten zeigt der Süßwasser-Abfluss von den Landflächen in den Ozean. Während Daten von ERA5 starke Abfluss Abnahmen über die letzten Jahrzehnte zeigen, deuten Beobachtungen auf leichte Zunahmen hin. Da der Abfluss in ERA5-Land, der offline Simulation von ERA5, deutlich höhere Werte zeigt, liegt das Problem wohl am Datenassimilationssytsem und insbesondere an der Einführung eines neuen IMS Schneeprodukts in 2004.

„The water that runs to the Arctic sea,

Ought to be balancing P-E.

While all of us know this has to be true,

Why then , we ask , are our budgets askew?

It‘s tough to assess the land ocean link,

When data on precip. and snowfall just stink.

It’s also hard to attain our goals

From streamflow records with numerous holes.

Rawinsonde data can help in this matter,

But estimates also contain ample scatter.

Is numerical weather prediction a cure?

Some of us think so, others aren’t sure.

Similar problems abound in the sea,

Where fluxes of fresh and salt don’t agree.

A Sverdrup here and a Sverdrup there,

Add it all up and it’s really a scare.

How do we measure the average rate

Of freshwater export out of Fram Strait?

And how do volumes of sea ice and brine

Affect the strength of the halocline?

The Atlantic inflow, where does it go?

Does the import have links with the NAO?

This is an issue that needs lot of thinking.

Likely combined with needed drinking.

To conclude, it seems that we still don’t know

Just how to balance the H2O.

But as the modeling crowd might say with inflection,

Lets try and do it without flux correction.“

- **Mark C. Serreze** (Lewis et al., 2000, p. 11-12)

1 Introduction

The Arctic plays an important role in the global climate system and is characterized through a unique landscape with close couplings between atmosphere, ocean and land, it's high surface reflectivity and low thermal energy, as well as the storage and discharge of freshwater and greenhouse gases (Tsubouchi et al., 2012, Serreze and Barry, 2014). This thesis examines the freshwater budget and the individual hydrological components of the Arctic atmosphere, Arctic lands and the Arctic Ocean.

The first complete freshwater budget for the Arctic Ocean is proposed by Aagaard and Carmack (1989) and updated by Serreze et al. (2006) and Dickson et al. (2007). However global climate change and consequential temperature increases lead to ongoing changes in the Arctic climate and hence also in the freshwater budget, making prevailing research necessary. Various studies show an intensification of the freshwater cycle, with changes arising in different hydrological components (e.g. Serreze et al., 2000; Peterson et al., 2002; Holland et al., 2006; Rawlins et al, 2010; Boisvert et al., 2015; Villamil-Otero et al., 2018; Box et al., 2019; Bitanja et al., 2020). Those changes in the Arctic large-scale freshwater budget entail local effects and also impact the global climate, e.g. through changes in the ocean circulation.

1.1 Aim of the work

Due to polar amplification surface warming in the higher latitudes exceeds the average global temperature change, having vast impacts on mass, energy and freshwater budgets. The Fifth Assessment Report of the Intergovernmental Panel on Climate Change (IPCC, 2013) states with *high confidence* that over the past two decades glaciers and the Greenland ice sheet have been losing mass, the Arctic sea ice has kept retreating and spring snow cover in the Northern Hemisphere has continued to decrease. With global mean surface temperatures continuing to rise it is *very likely* that those changes will continue through the 21st century. As freshwater plays a major role in the Arctic climate, an accurate and up-to-date analysis of the hydrological budget is from great interest.

Hence the purpose of this study is to assess the Arctic freshwater budget and examine the hydrological components on trends and interannual variabilities, using

primarily ERA5 reanalysis data. The period of consideration varies with availability of the used data, the considered area is described in the next section.

1.2 Definition and Physical Characteristics of the Arctic

The Arctic describes the area surrounding the North Pole and includes the Arctic Ocean, sea ice as well as the northern parts of North America, Europe and Asia. To the south there's no strict geographic boundary, in fact there are various different possibilities to define the Arctic area. The most formal definition takes the Arctic polar circle (66,57 °) as boundary. Nowadays this method is rather outdated, as Arctic conditions can be found far south of the Arctic circle. More often e.g. climatic criteria are used, such as the 10 °C July isotherm, or vegetational criteria, like the treeline. Depending on the area of application, also political regions or socio-economic factors can be used (Arctic Centre, n.d. *a*).

Figure 1 shows the Arctic boundary through polar circle, treeline and 10 °C July isotherm. Furthermore the classification into High-, Low- and Subarctic is made. The Arctic Ocean builds the bulk part of the area north of 70°N, and with the exception of a small gap between 20°E and 20°W it's almost entirely surrounded by land. The link between ocean and surrounding landmasses is remarkably strong, as the Arctic Ocean only accounts for about one percent of the global ocean volume, but obtains more than 10 % of the global river discharge.(Aagaard and Carmack, 1989)

The boundary of the Arctic used in this thesis is shown in figure 2. The Arctic Ocean is confined by borderlines with hydrographic gauging stations through the four major Arctic gateways: Bering Strait, Fram Strait, Davis Strait and the Barents Sea Opening. The total horizontal oceanic area enclosed by those gateways is 11.3×10^{12} m^2 (Jakobsson, 2002; Tsubouchi et al., 2012). The Arctic land area generally consists out of 64 catchment areas draining into the Arctic Ocean, building a terrestrial surface area of 17.4×10^{12} m^2. However in more detailed runoff analysis only the four largest basins Ob, Yenisei, Lena and Mackenzie are considered, with them accounting for about two thirds (Serreze and Barry, 2014) of total Arctic river discharge. The atmospheric component consists of the atmosphere overlying the oceanic domain and the land area, from the surface to the top of the atmosphere (TOA).

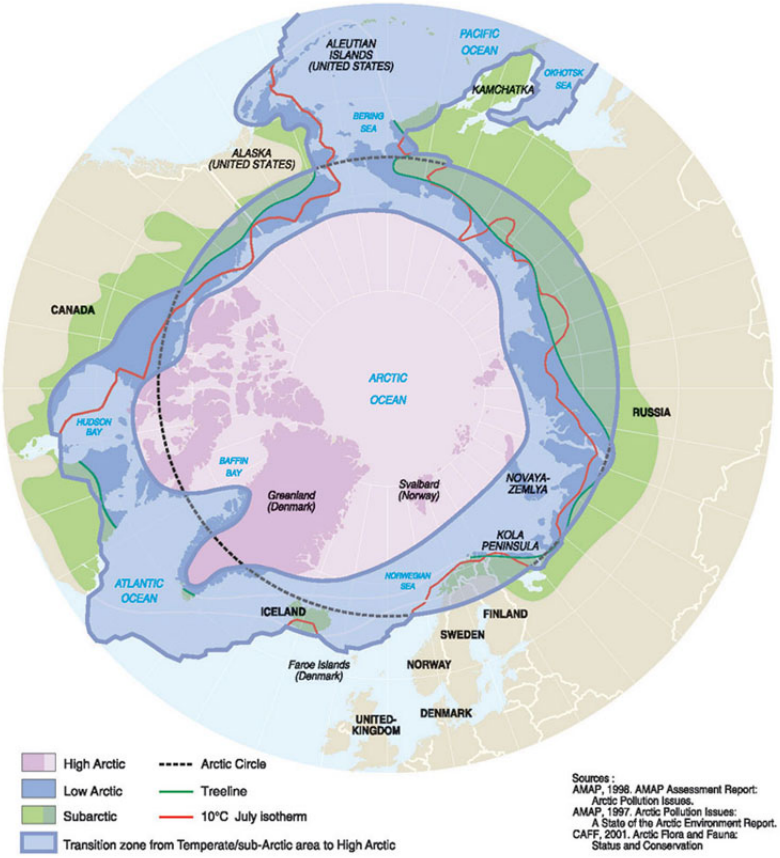

Figure 1: Boundary of the Arctic through Arctic Circle, Treeline and 10 °C July isotherm and classification into High-, Low- and Subarctic. (Figure taken from Arctic Centre, n.d.*b*)

1.2.1 Arctic Ocean

When not stated otherwise, this chapter is based on Serreze and Barry (2014). The surface layer of the Arctic Ocean consists of relatively fresh waters with 29 - 34 PSU (Practical Salinity Unit) and is separated by a strong halocline from underlying, saline, warmer waters. Due to the low water temperatures of the Arctic Ocean, the vertical density distribution is only dependent on salinity. Consequently the density of the low salinity surface layer is low and rises with depth, resulting in limited mixing of the ocean. The combination of low mixing, low salinity waters and low winter temperatures allows sea ice to form readily.

The low salinity surface layer is sustained by precipitation, by river discharge from the surrounding continents and by relatively fresh inflow from the North Pacific Ocean through Bering Strait. As mentioned above, more than 10 % of global river discharge

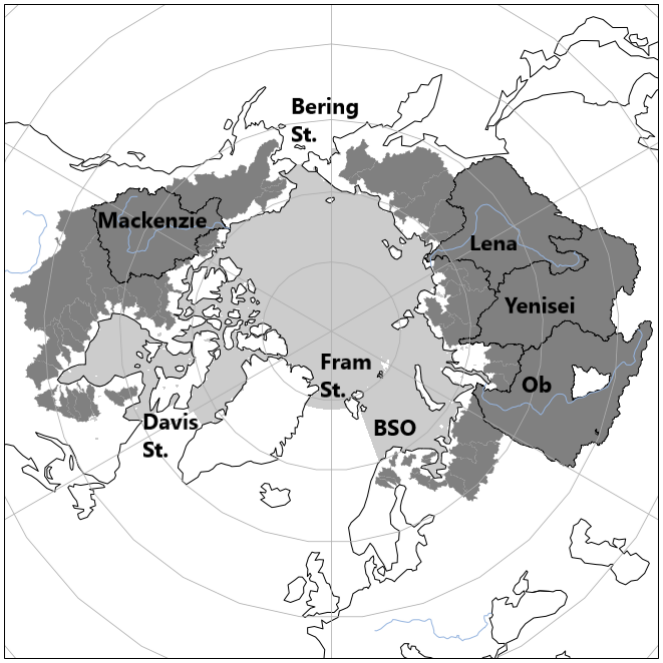

Figure 2: Area used in this study, including 64 terrestrial river basins and the Arctic Ocean bordered by lines with hydrographic gauging stations.

flow into the Arctic Ocean and with river discharge peaking in June due to terrestrial snow melt, big differences occur between summer and winter salinity. Salinity varies not only seasonally but also spatially, generally being lower in the vicinity of continental shelf and highest in the passage to the Atlantic Ocean. The Beaufort Sea for example features especially low salinity waters, due to it's proximity to Bering Strait and to the continental shelf and it's river outlets.

Furthermore the growth and melt of sea ice contribute to the salinity of the ocean. The decrease of sea ice in the past few decades, Arctic sea ice in September is declining at a rate of about 13 % per decade relative to the 1981 to 2010 average (NASA, 2020), leads to a decline of salinity.

Arctic Ocean Circulation The main currents of the Arctic ocean are shown in figure 3. Surface circulation is dominated on the one hand by surface winds that rotate surface waters (and overlying polar ice) in a large circle, the Beaufort Gyre, and on the other hand by the Transpolar Drift crossing the entire ocean from Siberia to Fram Strait. Deeper, warmer waters stream in from the North Atlantic Drift, are cooled in the Arctic Ocean and circulate in the North Polar Basin before flowing back into the

Atlantic Ocean (The Arctic System, n.d.). Exchange between Arctic waters and waters from the world oceans is limited and restricted to four straits:

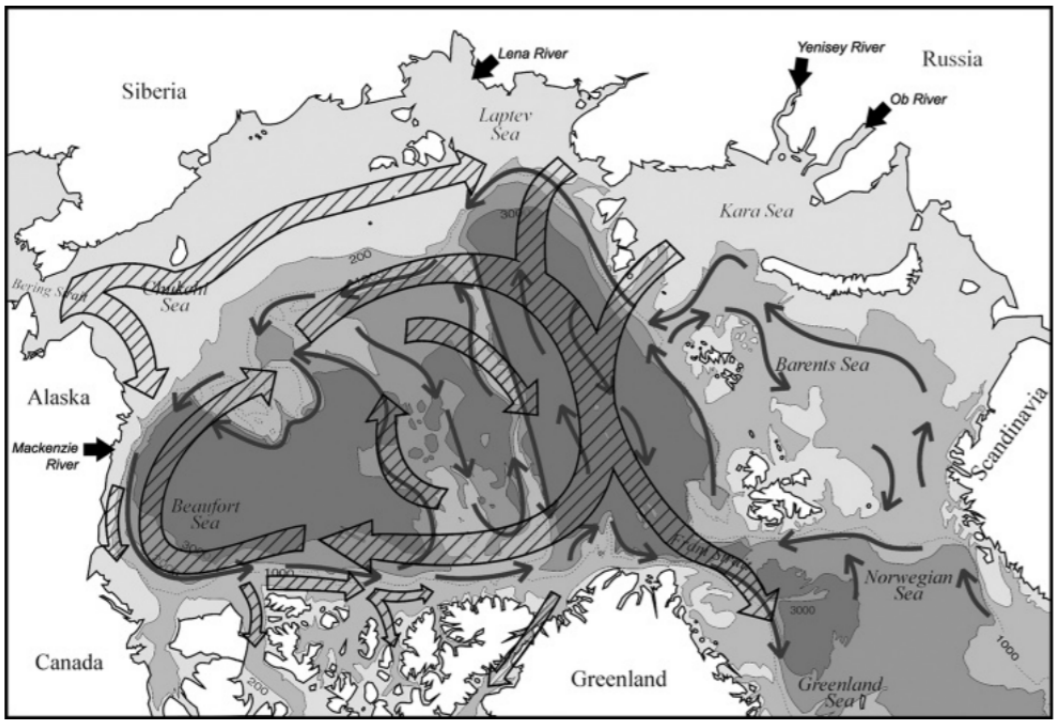

Figure 3: Major currents of the Arctic Ocean. Hatched arrows indicate surface currents and thin black arrows deep currents. Furthermore the location of the four major rivers draining into the Arctic Ocean is shown. (Figure taken from Serreze and Barry (2014); courtesy of G. Holloway, Institute of Ocean Sciences, Sidney, BC).

Bering Strait separates the Asian and North American continental shelfs and links the Pacific Ocean with the Arctic Ocean through a rather small (85 km wide) and shallow (50m deep) stream (Woodgate and Aagaard, 2005). The gateway is divided into two channels, with both channels transporting waters northward from the Pacific Ocean into the Arctic Ocean. Due to snow and ice melt, melting glaciers, river discharge and melting sea ice, the waters running through Bering Strait feature a relatively low salinity and hence build a source of freshwater for the Arctic Ocean. Due to it's lower density, freshwater stays atop the more salty deep sea water and contributes to sea ice formation. (Frontier Scientists, 2015)

Barents Sea Opening (BSO) is the pathway between Svalbard and Scandinavia. The Norwegian Atlantic Current, a northward extension of the Atlantic Ocean Current and the Gulf Stream, transports relative warm, saline waters from the Atlantic Ocean northward into the Arctic Ocean and divides into the BSO and the West Spitsbergen current, that builds a part of Fram Strait (Serreze and Barry, 2014). Due to the warmth of the water-masses flowing into the Arctic, large parts of the Barents Sea are kept ice free all year, leading to quite high heat and evaporation gradients between ocean and atmosphere (Smedsrud et al., 2013). Even though there are water-masses entering the Arctic Ocean through the BSO, due to it's high salinity, compared to a reference of 34.8 PSU, it counts as freshwater sink.(Serreze and Barry, 2014) The region of the Barents Sea - where warm, saline Atlantic water meets cold, fresh, Arctic water - is called polar front (The Arctic System, n.d.).

Fram Strait is the gateway between the eastern Greenlandic coast and Svalbard and is the only deep sea connection between the Arctic Ocean and the world oceans. It's divided into two currents, the West Spitsbergen Current transporting warm, saline waters from the Atlantic Ocean northward into the Arctic, and the East Greenland Current transporting relatively cold, fresh water southward out of the Arctic. The East Greenland Current consists about half half of fluid waters and sea ice and is responsible for about 90% of total sea ice export out of the Arctic Ocean. While technically an inflow, due to it's high salinity the West Spitsbergen Current counts as freshwater sink for the Arctic Ocean. (Serreze and Barry, 2014)

Davis Strait is the pathway between the west coast of Greenland and Baffin Island, part of the Canadian Arctic Archipelago (CAA). While the flow through the channels of CAA consists of many branches and strong currents and is difficult to monitor due to prevailing sea ice, almost the entire flow ends up exiting the Arctic through Davis Strait. In the eastern part of Davis Strait the northward flowing West Greenland Current transports relatively warm waters from the East Greenland Current, flowing around the southernmost point of Greenland, and from intruding waters from the North Atlantic Drift. In the western part of Davis Strait the Baffin Island Current transports relatively fresh Arctic waters and masses of ice southwards towards the Labrador Sea and the Atlantic. (NASA, 2002)

1.2.2 The Arctic Lands

Looking back at figure 1 the common subdivision of the Arctic into High Arctic, Low Arctic and Subarctic can be seen. High Arctic lands are generally characterized by more severe environmental conditions and shaped by tundra, the treeless region north of the Arctic treeline including polar deserts. The Greenlandic Ice Sheet covers an area of 1.71 million km^2 and builds the largest permanent ice mass of the Northern Hemisphere. In the Low Arctic 80-100 % of land is covered by plants, especially shrubs, sedges and grasses.The bulk part of the Arctic land area is underlain by perennially frozen ground, also known as permafrost. (Serreze and Barry, 2014)

Permafrost is present when ground remains continuously frozen through two or more consecutive years. The top layer in permafrost regions is called active layer and undergoes seasonal freezing and thawing. As permafrost controls the distribution, storage and drainage of surface and subsurface waters, it plays a major role for hydrological processes in the Arctic. Being an impermeable barrier permafrost prevents the vertical flow of water, blocking the infiltration of precipitation and meltwater to deep groundwater zones. This results in very wet, saturated soils and the building of lakes, unless drainage channels can form. In the case of sufficient drainage, the permafrost barrier leads to faster channelling of precipitation and meltwater. This again impacts river discharge and evaporation rates (Serreze and Barry, 2014). Not only the general presence of permafrost, but also the thickness of the active layer and the total thickness of the underlying permafrost are important factors for hydrological processes (White et al., 2007). Over the last 50 years climatic changes like air temperature, snow depth and length of the warm period, led to permafrost degradation and active layer thickening. Several areas have lost permafrost completely, especially along the southern permafrost boundary (Streletskiy, 2015).

Soil Moisture is the hydrological variable of the land surface with the strongest impact on moisture and energy fluxes like e.g. evaporation. Flat areas with a shallow active layer usually have quite high soil moisture content and relatively high evapotranspiration rates (White et al., 2007). Andresen et al. (2020) investigate changes in active-layer thickness and permafrost thaw and how they influence soil moisture and hydrology

projections by comparing various common land models. They find that despite models projecting warmer temperatures and increases in the net air–surface water flux (precipitation minus evapotranspiration), most models also project long-term drying of the surface soil in permafrost areas. As the active layer deepens moisture soaks into deeper soil layers, thus the surface soil gets dryer.

Snow Cover is present on most of the Arctic land and perennial sea ice for at least 6-8 months annually (Serreze and Barry, 2014) and is a key element in the global climate system, having strong impacts on energy and moisture budgets. Hydrological processes are affected through the direct water storage of snow in winter and its release as river discharge in spring and summer. Only slight shifts in timing, duration and thickness of snow cover affect the seasonal and yearly runoff characteristics (White et al., 2007). Studies show that high latitude regions experience earlier snowmelt onset in spring due to higher average winter and spring temperatures (Semmens et al., 2017; Foster et al.,2008), resulting in changes of spring runoff.

Lakes and Rivers: Lakes make out a large part of the Arctic and subarctic landscape and are strongly altered by changes in permafrost. Through the degradation of permafrost, and hence accumulation of water, lakes may increase in size. However when deeper permafrost thaws it allows internal drainage to the groundwater and thereby lakes may also decrease in size. (White et al., 2007)

Additionally the Arctic contains some of the largest rivers and drainage basins on Earth. Alone the four largest drainage basins, namely Ob, Yenisei, Lena and Mackenzie river, contribute about 68 % of total river discharge to the Arctic Ocean (Serreze and Barry, 2014).

Yenisei River is the largest Siberian river discharging into the Arctic Ocean. It rises in northern Mongolia and discharges into Kara Sea. With a maximum length of 5940 km and a basin size of 2.58 million km^2, it is the fifth largest river in the world (Davidson N.C.,2016). According to Holmes et al. (2013) the mean annual discharge of Yenisei River reaches about 673 km^3/year, Serreze and Barry (2014) obtain a mean annual runoff of 239 mm/yr for the period 1960 to 1998, equivalent to a discharge of 617 km^3/yr.

Lena River is the world's 11th largest river with a length of 4400 km and a catchment

area of 2.50 million km^2. The river rises on the Baikal ridge and discharges into the Laptev Sea (Degtyarev, 2016). Holmes et al. (2013) obtain a mean annual discharge for Lena River of about 588 km^3/year, Serreze and Barry (2014) estimate mean annual runoff to be about 221 mm/yr or 539 km^3/yr for the period 1960 to 1998.

Ob River is the third largest Siberian river emptying into the Arctic, with a length of 3650 km and a basin size of about 2.98 million km2. It rises in the Altai Mountains and discharges into the Arctic Ocean via Kara Sea (Yang et al., 2004a). According to Holmes et al. (2013) the mean annual discharge of Ob River reaches about 427 km^3/year, Serreze and Barry (2014) detect a mean annual runoff of 138 mm/yr for 1960-1998, equivalent to a discharge of 415 km^3/yr.

Mackenzie River rises in the Columbia Ice-field in Jasper National Park and discharges to the Arctic Ocean via the Beaufort Sea. With a length of 4240 km and a basin size of about 1.8 million km^2 it's the largest river in Canada and the second largest in North America (Robinson, 2019). Mean annual discharge reaches around 308-316 km^3/year (Holmes et al., 2013; Serreze and Barry, 2014).

1.3 Modes of Atmospheric Variability

The Arctic region is affected by various large-scale modes of atmospheric variability. The biggest impacts in the Arctic are due to the North Atlantic Oscillation (NAO) and its more comprehensive counterpart the Arctic Oscillation (AO), but also the Pacific North American (PNA) teleconnection and the Pacific Decadal Oscillation (PDO) influence the Arctic climate. NAO, the Atlantic side component of AO, describes the covariation in the strengths of the subpolar low near Iceland and the subtropical high near the Azores, while AO describes a shift of atmospheric mass generally between Arctic and mid-latitudes. Positive NAO/AO values characterise less mass than normal in the Arctic and more mass than normal in mid-latitudes, and vice versa for negative values. NAO/AO impact the Arctic climate and affect for instance surface air temperature, ocean heat transport, sea ice conditions, as well as hydrological parameters such as precipitation and moisture flux divergence. (Serreze and Barry, 2014)

Serreze et al. (1997) examined the connection of NAO and cyclone activities for the period from 1966 through 1993 and find a distinct poleward shift in cyclone activity

and hence a significant increase north of 60° during positive NAO phases. They find that under positive NAO extremes cyclone events at the climatological centre of the Icelandic Low are more than twice as common and significantly deeper than at negative NAO extremes. Phases of NAO and AO and their impacts on the hydrological cycle are examined further in section 4.2.1.

2 Arctic Hydrological Budget

Freshwater exists in three phases, namely as liquid water, solid ice and as gaseous steam. All three phases are active in the Arctic climate system and interact with each other. Transition between the phases is possible through freezing, melting, condensation, evaporation and sublimation. (Hantel and Haimberger, 2016)

The freshwater budget of the Arctic consists of three tightly linked branches, the Arctic Ocean, Arctic Lands and the overlying atmosphere. Freshwater can be converted within one of the branches and transported between all three of them. Figure 4 shows the three branches and the processes among them, as well as the flow through the Arctic boundaries.

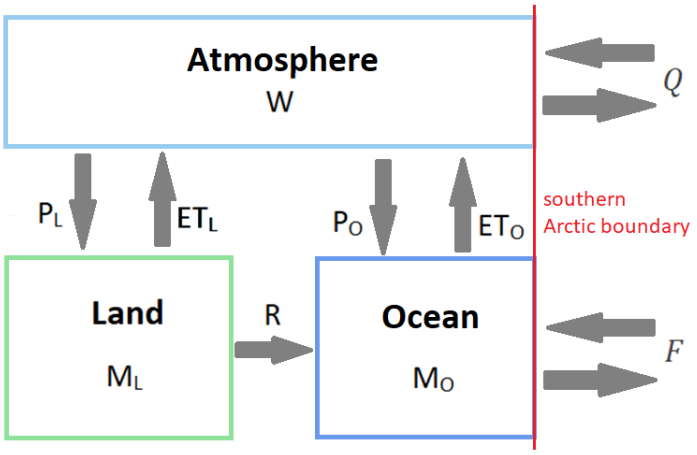

Figure 4: Freshwater fluxes and storage terms for the three Arctic branches atmosphere, land and ocean.

The atmosphere loses water to land and ocean through precipitation(P) in liquid (rain) and solid (snow) form, that is countered by part through evapotranspiration (ET). The difference of precipitation and evapotranspiration gives the net input of water from the atmosphere to the land and ocean surfaces, the net precipitation. Due to

the latitudinal variability in the suns incoming radiation, unlike at equatorial latitudes, in the Arctic in general P-ET is positive, with precipitation exceeding evapotranspiration. Excess water over the land domain, through processes like precipitation or snowmelt, gathers in rivers and flows into the ocean building another important variable in the hydrological budget, namely runoff R. As the Arctic domain is not a closed box, water is also transported through the Arctic boundaries. Q is the atmospheric horizontal transport of water vapour through the southern Arctic boundary and F is the oceanic freshwater transport through the Arctic gateways. Furthermore all three domains feature a storage component. While storage in the atmosphere is very short lived with a mean residence time of about a week, freshwater in the Arctic Ocean has a mean residence time of about a decade, being stored as liquid water and as sea ice (Serreze and Barry, 2014).

2.1 Hydrological Budget - Components

2.1.1 Precipitation

Accurate precipitation estimates for the Arctic area are difficult to obtain, with the station network in the Arctic being quite sparse, significant gauge undercatchment of solid precipitation, especially in high wind conditions, and satellite and reanalysis precipitation having rather large biases (Serreze and Barry, 2014). Serreze and Barry (2014) use a combination of station data sets, bias corrected NCEP/NCAR reanalysis fields and satellite-derived data to obtain precipitation estimates for the Arctic sector: In eastern Eurasia, northern Alaska, northern Canada and the central Arctic Ocean, winter is rather dry, while the Atlantic sector shows much higher winter month precipitation totals due to frequent cyclone activity along the North Atlantic cyclone track and orographic uplift of moist air-masses along the coasts of Scandinavia and eastern Greenland. Also the Pacific side shows higher winter precipitation values, due to the East Asian storm track and orographic effects. In summer, when the primary storm tracks are weakest, the highest precipitation totals are still found in the Atlantic and Pacific sectors. But also the land areas show their annual precipitation maximum in summer, due to terrestrial cyclone activity being highest in summer months, high evapotranspiration rates following the snowmelt season and convective precipitation.

Jakobson and Vihma (2010) assessed the Arctic atmospheric moisture budget using ERA-40 reanalysis. For the most part precipitation fields agree well with the results from Serreze and Barry (2014), however the regions with precipitation minima are shifted further into the Arctic Ocean, while NCEP/NCAR minima are rather centred over Candaian Arctic Archipelago.

Hurley (2014) compared Arctic precipitation fields from ERA-Interim, CFSR (Climate Forecast System Reanalysis) and MERRA (Modern Era Retrospective Analysis for Research and Applications). Overall all three reanalysis products reproduced similar precipitation patterns like NCEP/NCAR as described above (Serreze and Barry, 2014). Also monthly fields of long-term trends seem in good agreement across the three reanalyses datasets, with an exception of the northern North Atlantic sector (i.a. Fram Strait and the Norwegian Sea), where ERA-Interim data shows negative trends and anomalies (calculated as difference between 2001-2010 minus 1979–2010) while MERRA and CFSR show distinct positive anomalies. Wang et al. (2019) assessed and compared total precipitation and snowfall fields from ERA-Interim and ERA5 reanalysis and compared them with buoy observations from 2010 to 2016. Both total precipitation and snowfall are higher in ERA5 than in ERA-Interim in all seasons, with the largest differences occurring in the Atlantic sector.

As the climate warms, the hydrological cycle, and thus also precipitation, is going to intensify. This process is related to the ability of the warmer atmosphere to hold more water as defined by the Clausius–Clapeyron relation (Rawlins et al., 2010). Available observations and reanalysis datasets agree, that annual precipitation increased during the past decades, with the largest changes occurring in the cold season (Serreze et al., 2000; Rawlins et al, 2010; Rapaic et al., 2015; Box et al., 2019). According to Allen and Ingram (2002) the Clausius-Clapeyron relation yields a precipitation increase of about 6.5% per degree of warming. Bintanja and Selten (2014) use simulations from 37 state-of-the-art global climate models (within the *Coupled Model Intercomparison Project - Phase 5* (CMIP5)) for the period 2006-2100, and find an Arctic mean precipitation sensitivity of 4.5% per degree of warming. They attribute the changes in Arctic precipitation mainly to intensified local surface evaporation resulting from sea ice retreat and, to a lesser degree, to amplified moisture inflow.

2.1.2 Evapotranspiration

Evapotranspiration (ET) is the combination of surface evaporation and plant transpiration and is equivalent to the latent heat flux. Serreze and Barry (2014) describe the seasonal changes of ET using ET fields from MERRA (Modern Era Retrospective Analysis for Research and Applications) reanalysis for the four mid-season month January, April, July and October. During January MERRA shows low ET values over the ice covered Arctic Ocean and Arctic land areas. For a large part of the land areas, values are even negative, implying the transition from vapour to solid phase, however observations and models (Walsh et al., 1998) rather point to sublimation playing the key role. Maximum January ET values are found over the Norwegian Sea (locally more than 100 mm), where open water is overlain by a dry and cold atmosphere. In July ET peaks over land areas reaching values of up to 120-160 mm, while ET over the melting sea ice surface stays low. Due to smaller vertical humidity gradients and weaker winds ET values over the Norwegian Sea are lower than in winter. The seasonal evapotranspiration fields from ERA-40 (Jakobson and Vihma, 2010) show a similar pattern, with evaporation minima occuring over the Arctic Ocean, Greenland and partly over land areas in winter, and the highest evaporation values arising over the northern North Atlantic in winter and over the warmed landmasses in summer. Compared to observed values, Serreze et al. (2006) found ERA-40 evapotranspiration over the Arcitc land regions to be about 20-50 % to high, and stated that instead of the use of direct ET from reanalyses, the best estimate would be to calculate ET as a residual from observed precipitation and divergence of water vapor flux from ERA-40. This so-called aerological approach is discussed further in the next section and in section 2.2.1.

Boisvert et al. (2015) use moisture flux rates produced by Atmospheric Infrared Sounder (AIRS) data and find that ET rates from the Arctic Ocean have increased by 7% of the average annual Arctic evaporation in the period of 2003-2013. With the largest changes occurring during spring and fall in the Arctic coastal seas, due to sea ice melt and increased Sea Surface Temperatures (SSTs). One important contributor to increasing surface ET rates, especially in winter and late fall, is the retreat of sea ice, as open water areas at the freezing point lead to a lot higher ET values than ice areas with temperatures far below zero. (Serreze and Barry, 2014; Boisvert et al., 2015)

2.1.3 Net Precipitation

Net precipitation is the difference between precipitation and evaporation (P-E) and represents the local freshwater net input to the surface (Walsh et al., 1998). P-E marks one of the key variables in hydrological analyses, but due to the challenges in measurement of P and E, the direct difference of those two variables isn't always practical. Another approach of estimating P-E is the so called aerological approach, that makes it possible to obtain P-E without direct measurement of those two variables and involves calculation of the horizontal moisture flux into an atmospheric column (Serreze and Barry, 2014; White et al., 2007). More details about the aerological approach are given in section 2.2.1.

Cassano et al. (2007) compare three reanalysis datasets and global climate system models (GCSMs) for the period 1991–2000 and find positive annual P-ET values for the area north of 66.5° and over the Yenisei, Ob, Lena, Mackenzie and Yukon basins, indicating a freshwater flux to the surface. Typical values of annual net precipitation are 150–300 mm over land areas, 150–200 mm over the central Arctic Ocean and more than 1000 mm in the vicinity of the Icelandic Low (Serreze and Barry, 2014). In summer, as precipitation peaks over land, terrestrial ET rates are quite high resulting in small, or even negative P-E values.

Groves and Francis (2002) combined Sea level pressure and upper-level wind fields from the NCEP/NCAR Reanalysis with satellite (TOVS,TIROS Operational Vertical Sounder) retrieved fields of precipitable water to produce moisture transport and net precipitation datasets over the Arctic Ocean for the period of 1980 to 1998. They find summer P-E dominating the annual pattern, with it being twice as big as winter P-E. Further they find statistically significant increases of winter P-E in the Beaufort Sea and the eastern Greenland-Iceland-Norwegian Seas, and decreases in the Canadian Archipelago and Kara Sea, resulting in a slight increase for the whole Arctic Ocean. Additionally the authors connected P-E to the Arctic Oscillation, with P-E over the entire Arctic being 29% larger (20% lower) than average at positive (negative) AO phases.

Net precipitation over the Arctic ocean from the Japanese 25-yr Reanalysis (JRA-25) shows no significant trend for the period 1979-2007 (Rawlins et al., 2010).

Simulations with General Circulation Models (GCMs) indicate future increases in

Arctic P and ET, with trends in P generally being larger than those in E, resulting in increased net precipitation and thus increased freshwater delivery to the land surface (Holland et al., 2006; Rawlins et al., 2010). Cassano et al. (2007) use output from 15 global climate system models and 2 global reanalyses to analyse and predict changes in Arctic P-ET and find an increase in net precipitation during the 21st century over the central Arctic and the large river drainage basins. For the area north of 66.5° they find an increase in annual P-ET of over 20%. Further Cassano et al. (2007) create synoptic climatologies and derive a method to assess thermodynamic and circulation based changes in P-ET. They find that more than 75% of the projected change in 21st century is due to thermodynamic changes (= independent of changes in circulation), with dynamic changes (= due to changes in the frequency of occurrence of different synoptic patterns) being the next largest contributor.

2.1.4 Moisture Storage - Precipitable Water

Due to the low Arctic temperatures, the amount of atmospheric moisture is quite limited. The total column water vapor (=precipitable water PW) north of 70°N reaches about 2.5 mm in January and 14 mm in July (compared to a global average of 25 mm), with 95 percent of the moisture arising below 500hPa (Serreze, Barry and Walsh, 1995). In summer the distribution of PW is essentially dependent of latitude, in winter the spatial pattern shows great asymmetries. The highest values arise over the Norwegian Sea and the lowest values over the Canadian sector, resulting from evaporation patterns and vapour transports by synoptic-scale eddies (Serreze and Barry, 2014).

As the lower atmosphere in the Arctic is commonly nearly saturated, the amount of PW is closely linked to temperature changes, with PW increasing when the atmospheric temperatures increase. Furthermore PW is affected by horizontal and vertical (e.g. evaporation) moisture fluxes (White et al., 2007).

Both NCEP/NCAR, as well as ECMWF reanalysis data show no significant trends in annual PW over the Arctic area north of 60° in the late 20th century (Wang and Key, 2005; Serreze et al., 2006; White et al 2007). However isolating the Arctic Ocean, Wang and Key (2005) find PW decreases in winter and increases in spring, summer and fall. Satellite sounder retrievals for the period 1979 to 2005 show an PW increase of 5-10% during spring and summer, while in winter and autumn PW declined over

terrestrial regions and increased over the Arctic Ocean (White et al., 2007).

2.1.5 Atmospheric Moisture Transport

An important source of moisture for the Arctic region is the atmospheric horizontal transport of water vapor. Moisture circuits the North Pole counter clockwise and converges from lower latitudes into the Arctic region where it reaches the surface through precipitation, making it possible for the Arctic to keep producing sea and glacier ice through an adequate water supply (Hantel and Haimberger, 2016). The highest poleward moisture fluxes arise over the North Atlantic and North Pacific, with them contributing about 57% and 32% to total moisture flux (Villamil-Otero et al., 2018).

Changes in the strength of the meridional moisture gradient or changes in meridional wind can lead to changes in the horizontal moisture flux (White et al., 2007). Analysis of rawinsondes, satellite data and reanalyses suggest a strong link between the poleward moisture flux and large scale circulation patterns such as NAO and AO (Dickson et al., 2000; Rogers et al., 2001; Groves and Francis, 2002; White et al., 2007). Dickson et al. (2000) compared the mean winter meridional moisture flux across 70°N to moisture fluxes with extreme positive NAO phases and extreme negative NAO phases for the period 1974-1991. They find great differences between positive and negative NAO extrema, with the poleward moisture flux in the Nordic Seas being higher for positive NAO events (=strong Icelandic Low) and peaking to the west of Greenland at negative NAO events. Furthermore the southerly moisture flow over Canada is more pronounced during positive NAO events. Similarly to Dickson et al. (2000), Groves and Francis (2002) compared satellite derived moisture fluxes across 70° for positive/negative AO events in winter and summer. They also find northward moisture flux maxima in the Nordic Seas and stronger southward fluxes over Canada during positive AO events. With the atmosphere containing more moisture in summer, the annual signal is essentially dominated by moisture flux changes in summer.

Villamil-Otero et al. (2018) use NCEP/NCAR reanalysis to examine the poleward moisture flux across 60°N since 1959 and find an upward trend, that has been enhancing consistently since 1982. Those positive trends are found all year round, with August, September and November showing the highest trends. Further they link the upward trend in yearly moisture transport to an upward trend in cyclone activity since 1956

and find a positive correlation of 0.70 between poleward moisture transport and the cyclone activity index (CAI), a measurement for cyclone activity considering intensity, number and duration.

Zhang et al. (2012) compare atmospheric moisture transports, calculated from NCEP/NCAR wind and specific humidity reanalysis, with river discharge observations for 1948 to 2008 and find an intensification of poleward atmospheric moisture fluxes matching to increasing river discharges from the Eurasian watersheds in the past decades.

Using various state-of-the-art global climate model simulations, Bitanja et al. (2020) show that interannual precipitation variabilities will presumably increase during the 21st century due to changing fluctuations in poleward atmospheric moisture transport.

2.1.6 Runoff/River Discharge

While River Discharge and Runoff describe the same parameter, River Discharge is measured as water volume per unit time (e.g. m^3/s) and Runoff (e.g. m/s) is additionally divided by the contributing catchment area (Serreze and Barry, 2014).

River Discharge contains information about precipitation, evapotranspiration and water storage changes over the total catchment area above the gauging station, making it the ideal parameter to detect and measure changes in the terrestrial freshwater cycle. Containing some of the largest rivers and catchments, it's possible to monitor changes in the hydrological budget over a large part of the Arctic through discharge measurements in a relatively small number of rivers (White et al., 2007).

Various studies document long-term changes in Arctic river discharge, with the general trend of runoff numbers increasing for Eurasian rivers. Peterson et al. (2002) investigate long-term trends in discharge from the six major Eurasian rivers and find a 7% increase of average annual discharge to the Arctic Ocean from 1936 to 1999. Further they examine possible links between discharge trends and climate variability and find correlations with trends in global mean surface air temperature and the North Atlantic Oscillation.

Several studies find that the increasing runoff trend occurs mostly in winter and spring months (Lammers et al., 2001; Yang et al., 2002; Serreze et al., 2002; Peterson et al., 2002). Spring discharge increase is primarily attributed to early snowmelt due

to climate warming (Yang et al. 2002, 2003, 2004a; Serreze et al., 2002), while winter increase is perhaps associated with permafrost reduction and active layer thickening (Yang et al. 2002, 2004a; Serreze et al. 2002).Especially at the Lena River Basin, where permafrost underlies most of the catchment, with 77% being continuous (Holmes et al., 2013), permafrost and cryogenic effects are crucial for fluctuations in water discharge (Degtyarev V., 2016). Ye et al. (2003) find a runoff increase in winter, spring and summer months and a decrease in fall at the upper streams of Lena river, due to earlier snowmelt, climate warming and permafrost degradation. Also the other basins are affected by permafrost thaw with permafrost underlying 88% (33% continuous) of Yenisei basin, 82% (16% continous) of Mackenzie basin and 26% (2% continous) of Ob basin (Holmes et al., 2013). Increases in summer runoff at the lower Ob basin were linked to increases in summer precipitation and winter snow cover over the northern Ob catchment (Yang et al., 2004a).

Other studies emphasize the shift of discharge to low-flow winter months due to hydroelectric dams (McClelland et al., 2004; Yang et al., 2004a, 2004b).Yang et al. (2004a, 2004b) analyse monthly and yearly discharge records for 1936–1999 at the major sub-basins of the Yenisei and the Ob river to document streamflow changes induced by regulation systems. They find that mainly the upper portions of the Yenisei and Ob river basins are significantly altered by reservoir regulation, with peak discharge in the summer season being locally reduced by 15–30% for Yenisei and 10%–50% for Ob and a winter discharge increase of 5–30% at Yenisei and 25%–45% at Ob river (Yang et al., 2004a, 2004b). For Lena river Ye et al. (2003) find monthly discharge in the lower parts of the basin being significantly altered due to reservoir regulations. In the western part of Lena River (at Vilui valley) summer streamflow has been reduced by up to 55% and winter flows increased by up to 30 times. Those regulations, together with streamflow changes in the upper Lena basin cause strong discharge increases of up to 90% during low-flow months and also slight increases (5–10%) during the high flow summer month.

Thus because of human activities it's not easy to detect the hydrological response to climate change, using discharge data alone, as the discharge measured at the rivers outlet does not always represent natural changes and tends to underestimate streamflow trends in summer and overestimates the trends in winter (Yang et al., 2004a, 2004b).

In contrast to Eurasian rivers, several North American rivers showed small discharge declines. Dery and Wood (2005) analysed trends in 64 Canadian rivers for the period of 1964-2003 and found a 10% decrease (-22 mm/yr) in annual river discharge to the Arctic and North Atlantic Ocean, being entirely consistent with a observed decline in precipitation of 21 mm/yr between 1964 and 2000. Furthermore Dery and Wood (2005) find links between various large-scale modes of atmospheric variability (e.g. the Arctic Oscillation) and the total annual freshwater discharge in northern Canada.

Holland et al. (2006) perform simulations with General Circulation Models (GCMs) and find increasing trends in river runoff over the twentieth and twenty-first centuries. Main contributor to those trends is runoff from the Eurasian watersheds, with North American runoff playing an inferior part. For the twentieth century, the simulated increase in Eurasian runoff lies at 7%, agreeing with the changes observed by Peterson et al. (2002) for the period 1936 to 1999. Further they attribute the increase in Arctic river runoff in the twenty-first-century to positive P-E trends over the Arctic drainage basin, as soil moisture trends indicate that none of the extra P-E remains stored in the soil.

2.1.7 Oceanic sea ice and freshwater transport

As described in section 1.2.1 exchange with the Atlantic and Pacific Ocean generally takes place in four straits, with three straits (Fram, Davis and Bering) transporting, at least to some extent, freshwater and the BSO importing high salinity waters. Quantitative estimation of those freshwater fluxes is challenging, with observational data being rather sparse. To accurately quantify the fluxes, small-scale processes like recirculation have to be resolved, but common oceanographic gauging techniques are not able to obtain continuous data on small-scale horizontal resolution, leading to large uncertainties in flux calculations. Furthermore icebergs and processes like ridging hinder measurements. Thus most available estimates assume to some degree temporally and spatially stationary salinity fields. (White et al., 2007)

With the world warming the hydrological cycle is intensifying and thereby the freshwater fluxes from the Arctic Ocean to the North Atlantic are expected to strengthen. This could lead to a suppression of the rate of the Atlantic meridional overturning circulation, building one of the key aspects why an improved understanding in freshwater

exchanges between Arctic and Atlantic Ocean is so important. (Dickson et al., 2007)

Oceanic freshwater can be calculated relative to the mean Arctic salinity. The oceanic total water fluxes can be converted into ocean freshwater fluxes using a reference salinity REF. As reference usually the mean Arctic salinity is taken with 34.8 PSU (Serreze et al., 2006), but also slightly divergent values are common (e.g. Dickson et al.(2007) use a salinity of 35.2, representative for inflowing Atlantic water). Equation 1 shows the transformation of total water fluxes into freshwater fluxes.

$$FW = TW(1 - \frac{SAL}{REF}) \tag{1}$$

With freshwater flux FW, total water flux TW and observed salinity SAL. Hence a flux is a freshwater source/sink to the Arctic Ocean if the salinity of the total flux is less/greater than the reference salinity. (Serreze et al., 2006)

Serreze et al.(2006) combine data from several prior studies to estimate the oceanic freshwater fluxes relative to a reference salinity of 34.8 PSU. They find a net oceanic freshwater export of 9200 km^3 per year and an import of 8500 km^3 per year excluding the Canadian Arctic Archipelago. Dickson et al. (2007) extend the Arctic area further south to include Hudson Bay and the Nordic Seas and find a freshwater export of 9500 km^3 per year and a sum total freshwater flux of 4725-7515 km^3 per year.

An alternative way of freshwater flux estimation is through calculation of the salt mass fluxes. The following derivation is based on Bacon et al. (2015). The mass flux of the Arctic Ocean can be written as followed:

$$\underbrace{\iiint \frac{\partial \rho}{\partial t} dV}_{\dot{M}} = \iint \rho v ds dz + F_m^{surf} \tag{2}$$

The term on the left hand side denotes the change of mass in the considered volume. The first term on the right hand side is the side boundary mass flux of ocean waters and ice, with v being the ocean (and ice) velocity, and s and z being the horizontal and vertical coordinates. The last term is the surface mass flux consisting of precipitation, evaporation and runoff. Considering the flux of salinity S$\rho\mathbf{u}$, the last term in equation 2 is omitted, as there are no fluxes of salinity through the surface and the mass equation reads as followed:

$$\underbrace{\iiint \frac{\partial S\rho}{\partial t} dV}_{\dot{M}_S} = \iint S\rho v ds dz \tag{3}$$

Hence an imbalance between in- and outflow of salinity leads to a change in salinity storage $\dot{M}_S$. We are interested in the term on the right hand side of equation 3. Splitting S and ρv into means and anomalies and rearrangement yields an equation for salt/freshwater transports through the oceanic side boundaries:

$$FWT = \frac{\iint (\rho v)' S' ds dz}{\bar{S}} \tag{4}$$

For the whole derivation of equation 4 see Bacon et al. (2015) and Tsoubouchi et al. (2012, 2018). Technically speaking equation 4 denotes an equation for salt transports and has to be multiplied by (-1) to deliver freshwater transports.

Tsubouchi et al.(2012) estimate fluxes of freshwater and sea ice using an inverse box model and hydrographic observations that are present in the four main gateways since 2004 and find a net oceanic and sea ice freshwater flux of about 5897 +/- 1514 km^3 per year.

Fram Strait: Rabe et al. (2013) estimate liquid freshwater transports and their composition between 1998 and 2011 in the East Greenland Current in the Western Fram Strait using six hydrographic surveys and data from moored current meters. They find an average southward liquid freshwater flux of 3160 +/- 730 km^3 per year relative to a salinity of 34.9, consisting of about 130% water from rivers and precipitation, 30% freshwater from the Pacific, and a deficit of - 60% due to sea ice melt and brine from sea ice formation. Dickson et al.(2007) compare various studies and assume a total freshwater flux of about 5050 km3 per year, consisting of 2500 km^3/yr as ice and 2050–3000 km^3/yr as freshwater.

Davis Strait: Cuny et al. (2004) compute freshwater fluxes through Davis Strait using moored arrays from 1987-1990 and obtain a total freshwater flux of about 2900 +/- 1070 km^3 per year. Sea ice transport is estimated at 528 km^3 per year, building a way smaller ice flux than Fram Strait. Curry et al. (2010) estimate freshwater fluxes through Davis Strait from moored array data for the period 2004-2005 and find a flux of 3658 +/- 1290 km^3 per year relative to a mean salinity of 34.8 PSU. Azetsu-Scott et al. (2012) use chemical tracers as well as salinity and velocity fields from mooring arrays to asses and quantify freshwater fluxes through Davis Strait and their composition of sea ice meltwater, meteoric water and Arctic water in autumn 2004. They find a

total freshwater transport to the south of about 3784 km^3 per year, with the bulk part originating from Arctic waters, consisting of freshwater from the Pacific ocean and meteoric waters (mainly from Mackenzie River outflow). Melt and direct meteoric waters play rather an inferior part for the southward flux, but a northward freshwater flux of 350-1640 km^3 per year is mainly preserved due to meteoric water, especially glacial meltwater from the Greenland Ice Sheet.

Bering Strait: Woodgate and Aagaard (2005) estimate the inflow of freshwater through Bering Strait at 2500 +/- 300 km^3/yr, by using moored measurements as well as ship-based observations and considering the Alaskan Coastal Current, ice transports and stratification of the water column in the central Bering Strait.

Moored measurements show high interannual variability of freshwater, heat and volume fluxes through Bering Strait. Freshwater fluxes peak in 1998 (the start of continuous measurements) with about 2000 km^3/yr, then they decrease to about 1300 km^3/yr in 2001 and then increase again to 3000-3500 km^3/yr in 2011 (Woodgate et al., 2006; Woodgate et al., 2012). The increase between 2001 and 2011 is mainly due to a strong increase in volume fluxes, attributable by two thirds to an increase in the Pacific-Arctic pressure-head and one third to smaller local wind changes (Woodgate et al., 2012). Increased volume fluxes not only enhance freshwater inflow, but also increase heat fluxes, having significant impacts on the sea-ice cover, with the region of the Pacific inflow being the area with strongest ice-retreat in the Arctic (Woodgate et al., 2006).

With the data network being sparse, detection of long term trends and the effects of global warming on freshwater fluxes is difficult. Holland et al. (2006) perform model simulations and find a significant decrease of sea ice freshwater export over the twentieth and twenty-first centuries. The twentieth century alone brings a decrease in ice transports of 28%, caused mainly due to considerable thinning of the ice cover toward the end of the century. Just as trends in river runoff and net precipitation, those sea ice thinning and melt processes contribute to a freshening of the Arctic Ocean. This leads to an increased freshwater storage and results in a rise of freshwater export through Fram Strait and the CAA by 65% over the twentieth century and other 87% in the twenty-first century. Small increases in freshwater import through Bering Strait par-

tially compensate the enhanced freshwater outflow in the twentieth century, but are negligible over the twenty-first century due to a reduction of mass transport through Bering Strait. Thus not only decreasing salinity trends, but also changes in the oceanic circulation are necessary for changes in freshwater transportation. As the East Greenland Current and the CAA tend to speed up over the twenty-first century, the mass transport, and hence the freshwater export, rises. (Holland et al., 2006)

Condron et. al (2009) investigate the effects of NAO wind forcing on the oceanic freshwater transport through the Arctic gateways using a coupled ocean sea ice configuration of the MIT (Massachusetts Institute of Technology) general circulation model and find that the extent of the Beaufort gyre strongly influences changes in Arctic freshwater storage and fluxes. During negative NAO phases, anticyclonic high pressure leads to Ekman convergence and all freshwater stored in the Beaufort gyre being retained in the Arctic. In contrast, during positive NAO phases Ekman convergence in the Beaufort gyre is reduced through cyclonic circulation and freshwater export out of the Arctic accelerates, primarily via Fram Strait and the Canadian Archipelago.

2.1.8 Storage in Land and Ocean

Water can be stored at the land surface in different reservoirs, namely directly in the soil, as intercepted water in the canopy and in solid form as snow (Zsoter et al., 2020). Snow plays a significant role in seasonal storage, but can be neglected considering long term means. Interception is generally low and accounts only for a small part of the total water storage and hence is neglected in this thesis as well.

One of the driving forces for soil moisture is precipitation, and hence long-term trends of soil moisture are altered by interannual variations through large scale atmospheric variability like NAO and AO, just as precipitation itself (see section 4.2.1.). The other variable highly impacting soil moisture is temperature, as with rising temperatures soil moisture decreases. Sheffield and Wood (2007) analyse global and regional trends in soil moisture and droughts for 1950–2000. Especially in high northern latitudes they find a drying trend since the 1970s, caused, at least partially, by simultaneous temperature increases. And although precipitation, the primary driver for soil moisture, tends to slightly increase, the effect of temperature on soil moisture seems to have grown over the second half of the twentieth century, especially in northern latitu-

des. (Sheffield and Wood, 2007)

Freshwater in the ocean is stored in solid form as sea ice and in liquid form as low salinity surface waters with a mean residence time of approximately 10 years (Serreze and Barry, 2014). About three quarters of the total freshwater content are found in the upper 200m of the Arctic Ocean (White et al., 2007). With the hydrological cycle being intensified as the climate warms, the logical consequence would be a freshening of the Arctic Ocean, but several studies rather document the opposite and find a general decrease in freshwater content in the Arctic Ocean (e.g. Swift et al., 2004; Häkkinen and Proshutinsky, 2004). Steele and Ermold (2004) use observations along the Russian Arctic shelves to analyse long-term salinity trends since 1930 and propose that ocean salinities in those areas behave in anticorrelation with the NAO/AO, as they generally increased from 1930 to 1965 and then decreased again up to 1995. They suggest that wind forcing has a strong impact on salinity in the East Siberian Sea and Laptav Sea, as more westerly winds, that are connected to a high NAO/AO index, guide freshwater along the coast, while during low NAO/AO events more southerly winds force freshwater across the shelf toward the deep ocean. Additionally changes in atmospheric moisture flux convergence during NAO/AO phases impact local P-E and river discharge and hence salinity as well (Steele and Ermold, 2004; White et al., 2007). Steele and Ermold (2007) examined Russian dynamic height datasets from 1950 to 1990 and found that the Arctic Ocean lost about 30 cm of freshwater over that period, attributed to a faster acceleration of the freshwater export to the North Atlantic Ocean.

Annual component estimates Serreze and Barry (2014) estimate freshwater fluxes and storages at a reference salinity of 34.8 PSU (figure 5).

They find precipitation over the land domain exceeding evaporation by 2900 km^3 per year, providing runoff, the most important freshwater source for the Arctic Ocean. Runoff is estimated as 3200 km^3 per year. While precipitation provides the ocean about 3300 km^3 of freshwater per year, it's countered by an annual evaporation of about 1300 km^3. Positive fluxes of net precipitation over both, the land and ocean domain mean that the atmosphere constantly loses water. This has to be compensated by moisture fluxes over the Arctic boundary, estimated by Serreze and Barry (2014) as 4900 km^3/yr.

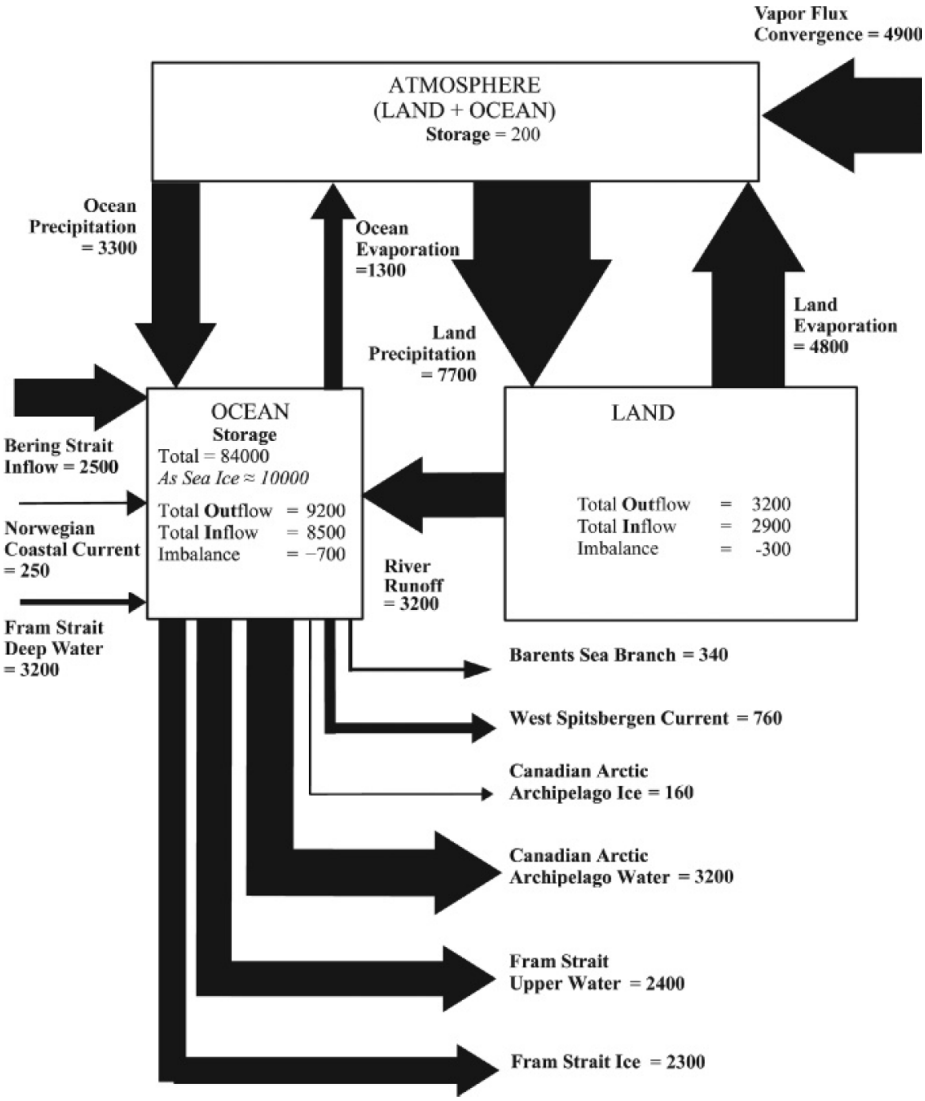

Figure 5: Mean annual Arctic freshwater budget, estimated relative to a reference salinity of 34.8 psu. Stores are in km^3 and transports are in km^3 per year. Taken from Serreze et al., 2006; Serreze and Barry, 2014

The Arctic Ocean gains about 2500 km^3/yr of low-salinity waters through Bering Strait. The major outflows are through Fram Strait (2400 km^3/y as low-salinity liquid water, 2300 km^3/y as sea ice) and through the Canadian Arctic Archipelago (3200 km^3/y as low-salinity liquid water). With a mean residence time of about a decade, freshwater storage in the Arctic Ocean is estimated at 84000 km^3. In the atmosphere, where water vapour has a residence time of only about a week, storage is estimated at 200 km^3.

2.2 Budget Equations

2.2.1 Atmosphere

Following the general, local transport theorem formulated in Hantel and Haimberger (2016), the transportation of water for an atmospheric column from the earth and respectively ocean surface to the top of the atmosphere (TOA), can be written as followed.

$$\underbrace{\frac{\partial q}{\partial t}}_{storage} + \underbrace{\nabla \cdot q\mathbf{V}}_{hor.\ flux} + \underbrace{\frac{\partial q\omega}{\partial p}}_{vert.\ flux} - \underbrace{Q^q}_{conversion\ rate} = 0 \tag{5}$$

With specific humidity q, the horizontal flux of specific humidity q$\mathbf{V}$ and qω the vertical flux. Q^q is the conversation rate from q into another phase. Integration of equation 5 in pressure coordinates yields:

$$\frac{\partial}{\partial t} \underbrace{\left(\frac{1}{g}\int_0^{p_s} q dp\right)}_{\substack{column\ water\ vapor \\ W}} + \nabla \underbrace{\left(\frac{1}{g}\int_0^{p_s} q\mathbf{V} dp\right)}_{\substack{horizontal \\ moisture\ flux \\ \mathbf{Q}}} + \underbrace{\frac{1}{g}\overline{q'\omega'}_{SFC}}_{\substack{evaporation\ rate \\ ET}} - \frac{1}{g}\int_0^{p_s} Q^q dp = 0 \tag{6}$$

The first term is the temporal change of total column water vapor W, the second term is the divergence of horizontal moisture flux Q and the third term is the vertical flux a.k.a evaporation rate ET. The last term of equation 6 represents the interaction of condensed water in the atmosphere. The small effects of phase change, represented by clouds and convergence of liquid and solid water, are neglected, in consequence the last term of equation 6 has to be precipitation P. So the freshwater budget for the atmosphere can be written as:

$$\frac{\partial W}{\partial t} = ET - P - \nabla \cdot \mathbf{Q} \tag{7}$$

Looking back at figure 4, equation 7 describes exactly the pictured situation. Water storage in the atmosphere W rises with evapotranspiration ET from the underlying surfaces and decreases with precipitation P. P and ET generally are not in balance, so assuming stationary conditions (=a timely constant storage term W) there has to be a moisture flux Q that transports water horizontally from or into the considered column.

Aerological approach: Rearrangement of equation 7 yields an equation for P-ET, with the last term, the time change of the columns precipitable water, being zero for long-term annual means and assuming stationary conditions:

$$P - ET = -\nabla \cdot \mathbf{Q} - \underbrace{\frac{\partial W}{\partial t}}_{\substack{=0 \ for \ long-term \\ annual \ means}} \tag{8}$$

The advantage in using the aerological approach is that the terms on the right side of equation 8 can be obtained from reanalysis through vertical profiles of specific humidity and winds, and hence the problems with direct measurement of P and ET as well as typical biases in surface variables from reanalysis can be avoided. (Serreze and Barry, 2014)

2.2.2 Land

For the land domain, horizontal moisture flux from the atmosphere has to be replaced by a horizontal transport of liquid water inside the land column. Water accumulates in surface and sub-surface rivers and discharges as runoff R into the ocean. So with runoff R and water storage in the land column M_L, analogy to equation 7, the budget equation for a land column can be written as:

$$\frac{\partial M_L}{\partial t} = P - ET - R \tag{9}$$

Contrary to the atmosphere, for land the signs of P and ET are reversed, with precipitation being a freshwater source and evapotranspiration a sink. Furthermore runoff builds another sink flowing out of the land domain into the ocean.

Considering shorter time scales, the parameters snowfall (SF) and snowmelt (SMLT) have to be considered, as they represent a seasonal storage component. That leads to equation 10:

$$SF - SMLT = P - ET - R \tag{10}$$

2.2.3 Ocean

Again, just as for land, evaporation from the oceans surface builds a freshwater sink and precipitation over the ocean domain a source. Another source is runoff from the

land area into the ocean and equally to the horizontal transport of moisture Q for the atmosphere, there's a lateral transport of liquid water and sea ice $\nabla \cdot \mathbf{F}$ through the boundaries of the oceanic domain. With M_O being the water storage inside the water column, the budget equation can be written as:

$$\frac{\partial M_O}{\partial t} = P - ET + R - \nabla \cdot \mathbf{F} \tag{11}$$

3 Data

3.1 Reanalysis

Reanalysis combines today's weather models and data assimilation systems with observations made in the past and delivers a globally and timely complete and consistent, three dimensional picture of the past Earth's climate system, including atmosphere, ocean and land surfaces. The advantage over time series of Analysis from Numerical Weather Models (NWP) is the use of the same model and data assimilation system through the whole process, guaranteeing a homogeneous time series.

3.1.1 ERA5 reanalysis

ERA5 is the latest ECMWF reanalysis product for atmosphere, ocean waves and land and marks the fifth generation of atmospheric reanalysis produced by ECMWF (Hersbach et al., 2020). Currently data is available from 1979 to present, with an extension back to 1950 being in progress. ERA5 uses 4-dimensional variational analysis (4D-Var) data assimilation in the CY41R2 cycle of ECMWF's Integrated Forecast System (IFS) and is coupled to a soil model (HTESSEL, described below) and an ocean wave model. ERA-5 produces data on a reduced Gaussian grid at a horizontal resolution of 31km and a temporal resolution of an hour, with monthly means being also available. It contains 137 hybrid sigma/pressure levels and spans through tropo-, strato- and mesosphere from the surface up to 0.01 hPa. There's also single level (surface) data available, such as 2m temperature, precipitation and vertical integrals over the entire atmosphere. (Hersbach et al., 2020, ECMWF, 2020*a*)

Data can be downloaded from the Climate Data Store (CDS) on regular latitude-

longitude grids at 0.25° x 0.25° resolution. Table 1 shows the parameters used in this study.

HTESSEL: The Hydrology Tiled ECMWF Scheme for Surface Exchanges over Land is the land-surface model of the ECMWF IFS and the improved successor of TESSEL (Tiled ECMWF Scheme for Surface Exchanges over Land). It's used to describe the state of the soil including vegetation and snow cover. Therefore grid boxes are split up into up to six tiles over land (bare ground, low and high vegetation, intercepted water, shaded and exposed snow) and 2 tiles over water (open and frozen water), all exhibiting different energy and water balances. Vertically it contains four layers, with the possibility of a single snow layer. To deal with precipitation an interception layer is used that accumulates precipitation until saturation is reached and the excess water is then divided into surface runoff and infiltration. Subsurface runoff is calculated by Darcy's law using a four-layer discretization with evaporation and infiltration at the top, free drainage at the bottom and additional water sinks through root extraction. While in TESSEL a single loamy soil was used, HTESSEL uses a spatially varying soil type and enables a varying surface runoff dependent on local topography and soil type. Hence two adjacent grid boxes with equal land surface conditions and receiving the same amount of precipitation, feature different amounts of surface runoff and soil water drainage proportional to the terrain complexity and soil texture class. (Balsamo et al., 2008)

3.1.2 ERA5-Land

ERA5-Land is the product of an offline HTESSEL simulation (Zsoter et al., 2020) and is produced by replaying the land component of ERA5 without coupling to the atmospheric module and the ocean wave model of the ECMWF's Integrated Forecasting System (IFS). Data assimilation is not used, observations affect the simulation only indirectly through the atmospheric forcing of ERA5. Those simplifications make it possible to run the simulation in a higher resolution. ERA5-Land produces data at a horizontal resolution of 9 km and a temporal resolution of an hour. (ECMWF, 2020*b*)

Data can be downloaded from the Climate Data Store (CDS) on regular latitude-longitude grids at 0.1° x 0.1° resolution from 1981 to present. Table 1 shows the para-

meters used.

3.1.3 ERA-Interim

ERA-Interim is the precursor of ERA5 and is available from 1979 up to August 2019. It includes 4D-Var data assimilation in the Cy31r2 cycle of ECMWF's Integrated Forecast System (IFS). The dataset contains 60 vertical levels, from the surface up to 0.1 hPa at a spatial resolution of 80 km and a temporal resolution of 6 hours. (Dee et al., 2011)

Figure 6 shows the main differences between ERA-Interim, ERA5 and ERA5-Land.

	ERA-Int	Era-Int/Land	ERA5	ERA5-Land
Period covered	Jan 1979 – NRT(*)	Jan 1979 – Dec 2010	Jan 1979 - NRT	Jan 1979 - NRT
Spatial resolution	~79km / 60 levels	79 km	~32 km / 137 levels	~9 km
Model version	IFS (+TESSEL)	HTESSEL cy36r4	IFS (+HTESSEL)	HTESSEL cy43r1
LDAS	cy31r1	NO	cy41r2	NO
Uncertainty estimate	-	-	Based on a 10-member 4D-Var ensemble at 62 km	Based a 10-member atmospheric forcing at 31 km
Output frequency	6-hourly Analysis fields	6-hourly Analysis fields	Hourly (three-hourly for the ensemble)	Hourly (three-hourly for the ensemble)

Figure 6: Main differences between ERA-Interim, ERA5 and ERA5-Land. From Muñoz-Sabater (2017)

3.1.4 ORAS 5

As historical observations are particularly sparse in the ocean, oceanic reanalysis systems are needed to deliver globally and timely complete fields of the past oceanic state. Those reanalysis fields are used i.a. for initialization of coupled forecasting systems.

ORAS5 (Ocean ReAnalysis System 5) is the latest ECMWF oceanic reanalysis product and is part of OCEAN5, the 5th generation of ECMWFs ocean and sea-ice ensemble (5 Member) reanalysis-analysis system (Zuo, 2018). It uses the ocean model NEMO 3.4 in the ORCA025.L75 configuration with 75 levels in the vertical and a horizontal resolution of 0.25°. To avoid polar singularities a tripolar grid is used. Figure

Parameter name	Abbreviation	Parameter ID
ERA5		
Surface latent heat flux	slhf	147
Total precipitation	tp	228
Vertical integral of divergence of moisture flux	viwvd	162084
Total column water vapour	tcwv	137
Sea surface temperature	sst	34
Mean sea level pressure	msl	151
Runoff	ro	205
Surface runoff	sro	8
Sub-surface runoff	ssro	9
Snowmelt	smlt	45
Snowfall	sf	144
Snow evaporation	es	44
Volumetric soil water layer 1	swvl1	39
Volumetric soil water layer 2	swvl2	40
Volumetric soil water layer 3	swvl3	41
Volumetric soil water layer 4	swvl4	42
ERA5-Land		
Runoff	ro	205
Surface runoff	sro	8
Sub-surface runoff	ssro	9
Snowmelt	smlt	45
Snow evaporation	es	44
Volumetric soil water layer 1	swvl1	39
Volumetric soil water layer 2	swvl2	40
Volumetric soil water layer 3	swvl3	41
Volumetric soil water layer 4	swvl4	42
ERA-Interim		
Surface latent heat flux		
Total precipitation		
Runoff		

Table 1: Parameters used from ERA5, ERA5-Land and ERA-Interim.

7 shows a schematic representation of the tripolar grid - two north mesh poles are placed over land and a grid is constructed out of embedded ellipses (pseudo latitudes) and its normals (pseudo longitudes) (NEMO, 2017). To consider the influences of sea ice, the dynamic-thermodynamic sea ice model LIM2 is used. Additionally observations of subsurface temperature, salinity, sea-ice concentration and sea-level anomalies are assimilated through 3DVAR-FGAT (Zuo, 2018). In addition time-varying forcing fields for ORAS5 are derived from ERA-Interim.

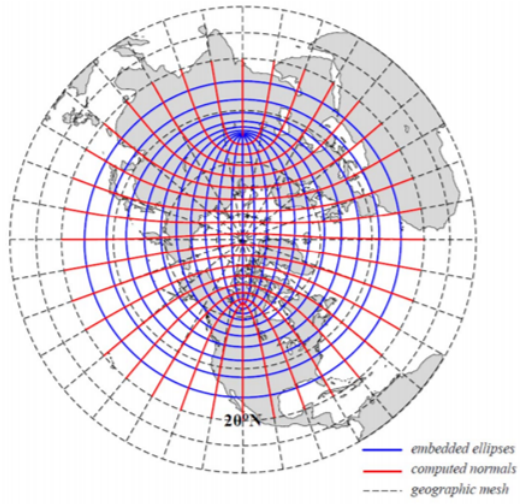

Figure 7: Tripolar grid from ORCA model configurations. Transition between a regular grid with two poles and the tripolar grid occurs at 20°N (NEMO, 2017).

3.2 GloFAS-ERA5 global river discharge reanalysis

Direct measurement of river discharge and/or runoff into the Arctic basin is hardly feasible, due to i.e. river icing. This lack of observations, both in time and space, is present in many parts of the world making the estimation of past, present and future hydrological conditions to a key challenge in hydrology. While reanalyses build an advancement, they are currently not ideal for many hydrological applications producing runoff output at each grid cell and not at catchment scales directly. The Global Flood Awareness System (GloFAS) solves this problem by combining runoff from the HTESSEL land surface model from ERA5 with the LISFLOOD hydrological and channel routing model. GloFAS, an operational system for monitoring and forecasting floods, was developed by the Joint Research Centre (JRC) of the European Commission, the University of Reading, and the ECMWF. As part of GloFAS also a long term, near real time river discharge reanalysis is produced. It's a global, gridded dataset with a horizontal resolution of 0.1° and a daily temporal resolution. The dataset is available from 1979 until near real time. Figure 8 shows a schematic illustration of the key components in the GloFAS-ERA5 river discharge reanalysis dataset. (Harrigan et al., 2020)

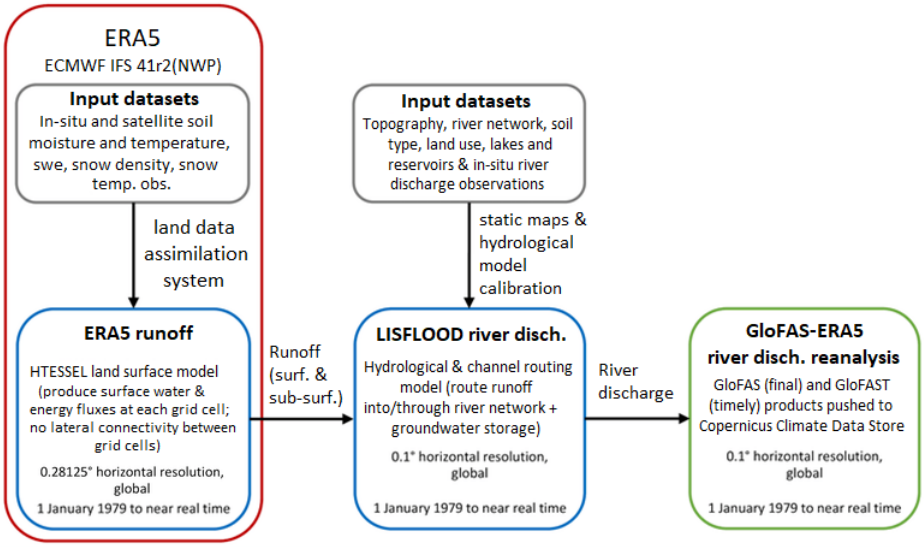

Figure 8: Schematic structure of GloFAS river discharge reanalysis (Harrigan et al., 2020).

3.3 Discharge Measurements

Observing records vary among the various countries and rivers with the longest time series coming from Russia, where discharge monitoring began in the mid 1930s. In contrast discharge measurement in North America did not begin until the 1970s (1973 for Mackenzie River) (Holmes et al., 2018). The data used in this study comes from Roshydromet (Ob, Yenisei and Lena) and from the Water Survey of Canada (Mackenzie) and was downloaded through the Arctic Great Rivers Observatory (Shiklomanov, 2020). ArcticGRO analyses the chemistry and discharge of Arctic rivers, focusing on the six largest Arctic rivers (Ob, Yenisey, Lena, Kolyma, Yukon and Mackenzie) which account for 67 % of the pan-Arctic watershed area. Next to measurements of biogeochemical parameters, ArcticGRO monitors daily discharge data, which are available for free through ArcticGRO's website (arcticgreatrivers.org) and through the Arctic Data Center. Figure 9 shows the position of the used gauging stations. For Ob River discharge is measured at Salekhard (66.63°N, 66.60°E), for Yenisei River at Igarka (67.43°N,86.48°E), for Lena River at Kyusyur(70.68°N,127.39°E) and Mackenzie River at Tsiigehtchic (67.45°N,133.74°W).

Figure 9: Position of the gauging stations Ob-Salekhard (66.63°N,66.60°E), Yenisei-Igarka (67.43°N,86.48°E), Lena-Kyusyur (70.68°N,127.39°E) and Mackenzie-Tsiigehtchic (67.45°N,133.74°W)

3.4 Oceanic flux measurements - ArcGate

Due to it's unique geometry it's possible to enclose the Arctic Ocean by landmasses and hydrographic observation lines placed in the four major Arctic gateways. Those hydrographic lines consist of arrays of moored instruments measuring variables like temperature, salinity and velocity, making it possible to calculate fluxes of volume, heat and freshwater. Figure 10 shows the position of the hydrographic lines in Bering Strait, Fram Strait, Davis Strait and BSO. (AWI,2019)

The ARCGATE project, funded as a EU Marie Curie project, was launched by the Alfred Wegener Institute (AWI) in the year 2015, with the purpose to efficiently use all the individual mooring arrays across the Arctic boundary in an attempt to calculate the above mentioned oceanic fluxes for the period of 2004 to 2010 (AWI, 2019). Therefore the Arctic Ocean is treated as a single box, bounded by the land masses of North America, Greenland and Siberia and the hydrographic lines through the Arctic gateways. One small gap in the Canadian Arctic Archipelago is not included in the box model directly, but the overall uncertainty of the fluxes is adapted by estimated transports from a six-week measurement campaign in early 1972. Vertically the box is bounded by the impermeable seabed at the bottom and the sea surface (or upper part of floating sea ice) at the top. The upper boundary allows exchanges of heat

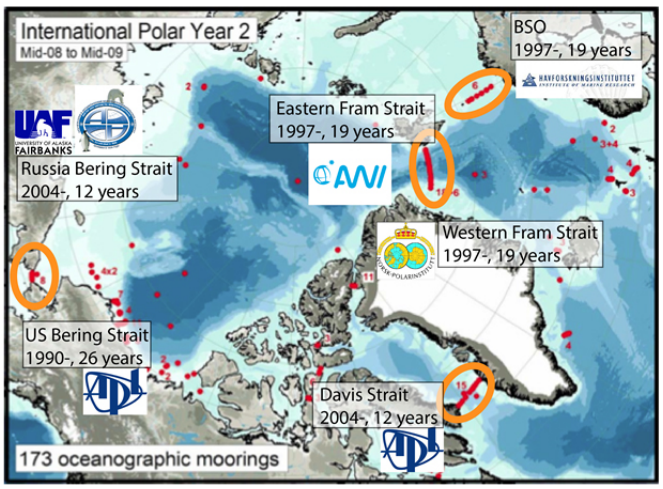

Figure 10: Placement of the hydrographic lines in the four gateways, length of the observations and operating research institutes.(AWI,2019)

and freshwater with the overlying atmosphere, like i.e. precipitation, evaporation or runoff. Furthermore storage of volume and freshwater are not permitted, as salinity-anomaly and volume are assumed to be stationary (Tsubouchi et al., 2012). Figure 11 shows the position of the moored instruments in the individual straits. In total there are 138 moored instruments distributed to 41 mooring sites, providing measurements of temperature, salinity and velocity (Tsubouchi et al., 2018). Especially in shallow

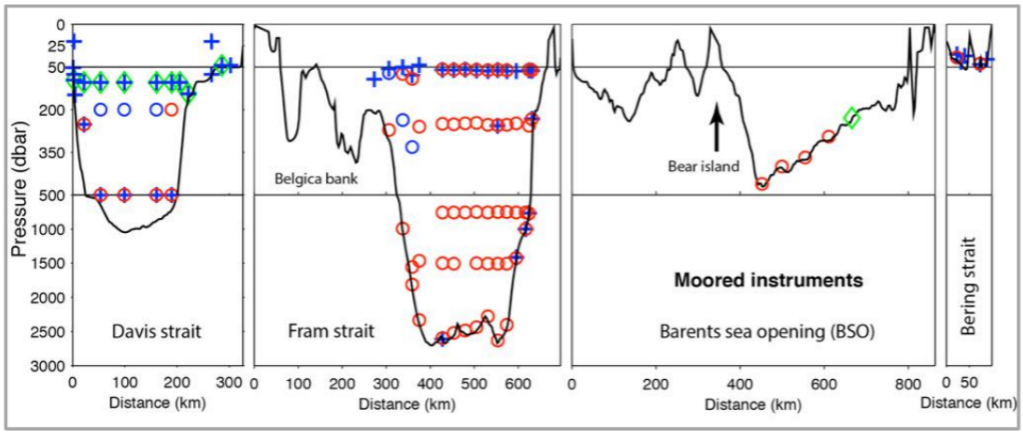

Figure 11: Vertical profiles of the mooring sites and locations of the moored instruments. Blue crosses are temperature and salinity measurements, blue circles are velocity and salinity measurements, red circles are velocity measurements and the green diamonds indicate measurements of velocity profiles (Tsubouchi et al., 2018).

waters, like Bjørnøya Bank between Svalbard and Bear Island, there are areas with

poor data coverage, mainly due to problems with sea ice. This is compensated by vessel-based hydro-graphic data and output from the NEMO ocean model, which is available to Tsubouchi et al. (2018) at a horizontal resolution of 3 kilometres and 75 vertical levels. Observation data are projected onto the model grid and through vertical and horizontal interpolation the complete cross sections of the individual straits are filled with data. The resulting fields of temperature, salinity and velocity are then averaged to obtain monthly fields and are used to calculate volume, heat and freshwater transports through the individual straits. (Tsubouchi et al. 2012, Tsubouchi et al. 2018)

4 Results

4.1 Atmosphere

4.1.1 Net Precipitation

Net precipitation (P-ET) is the only parameter present in all three hydrological equations (7,9,11) and one of the key factors in understanding the hydrological budget. Net precipitation is calculated out of total precipitation and evaporation from ERA-5 reanalysis. Total precipitation is the sum of convective and large-scale precipitation and includes liquid (rain) and frozen (snow) water. Not included are fog, dew and precipitation that evaporates before reaching the Earths surface. Even though the effects of transpiration in Arctic latitudes are quite small, evaporation does include a simplified representation of transpiration (CDS, 2019). As evaporation in ERA5 is defined positive towards the Earths surface (condensation), net precipitation is calculated as P+E, with E being negative for evaporation and positive for condensation.

Figure 12 shows mean evaporation, precipitation and calculated net precipitation from ERA5 for the period 1979-2018. Negative evaporation values mean an upward flow of water (=evaporation), while positive values stand for a downward flow of water (=condensation). Strong evaporation fluxes can be seen in the atmosphere overlying the land domain, coming from the warming of the landmasses in summer months, and at the Barents Sea. High values at Barents Sea are a consequence of warm waters entering the Arctic through the North Atlantic Current. Total annual precipitation is rather low over the bulk part of the Arctic Ocean. Highest precipitation values are found at mountainous regions as well as over the Atlantic Sector (mainly at the Barents Sea and the Norwegian Sea), due to the northward extension of the North Atlantic cyclone track and Icelandic Low as well as orographic uplift. Apart from the Barents Sea and terrestrial lower latitude regions, where annual net precipitation is slightly negative, the long-term annual means of net precipitation in almost the whole Arctic area show slightly positive values, meaning that over the year precipitation exceeds evaporation.

Serreze and Barry (2014) determine net precipitation using the aerological method and by interpolating rawinsonde data and receive values of 188 mm/yr (aerological) and 163 mm/yr (rawinsonde) for the area north of 70°N. Calculating P-ET out of

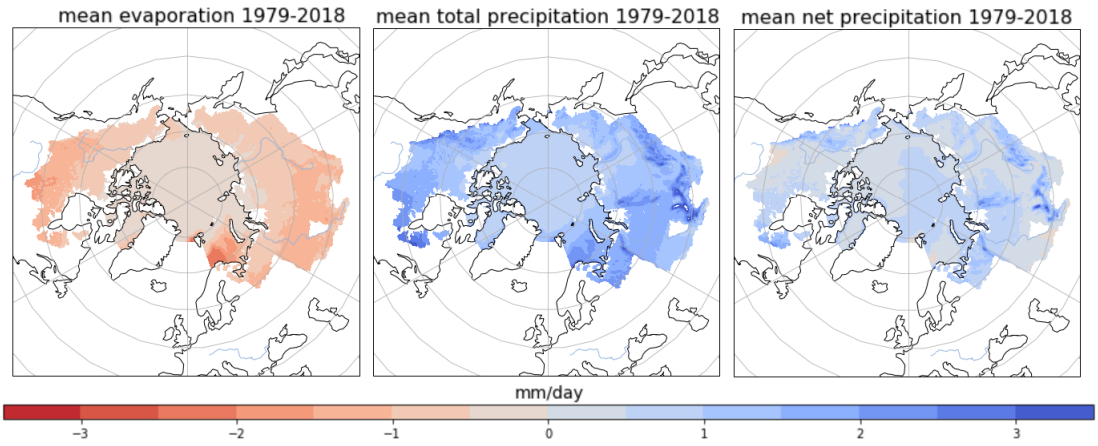

Figure 12: Mean ERA5 evaporation (left), precipitation (middle) and net precipitation (right) for the atmosphere overlying the considered oceanic and terrestrial domain. The mean is calculated over the period 1979-2018 and units are mm per day.

precipitation and evapotranspiration from ERA5 yields a value of 193 mm/yr north of 70°N and 213 mm/yr for the area used in this thesis.

4.1.2 Moisture flux

For long-term annual means the hydrological equation for an atmospheric column (equation 7) can be simplified by dropping the change of total column water vapour (the left side of the equation), hence the divergence of moisture flux and net precipitation should be in balance. Similar to figure 12 the long-term annual mean moisture flux divergence shows positive values over the ocean and land domain, representing vapor flux convergence. Looking at the field seasonally (figure 13), net precipitation and moisture flux divergence over the ocean are positive all year round, the only exception build Barents Sea and the Norwegian Sea, with slightly negative values in winter. As mentioned above those negative values are a consequence of high evaporation rates due to warm waters entering the Arctic through the North Atlantic Current.

In large parts of the terrestrial domain summer values are negative, as evaporation exceeds precipitation due to the summer warming of the land areas. Meanwhile positive values arise mostly at mountainous areas, where precipitation is high due to orographic effects and convection.

The mean annual cycles of P, ET, P-ET, moisture flux divergence and total column water vapour from ERA5 are shown in figure 14 separately for the ocean and the land

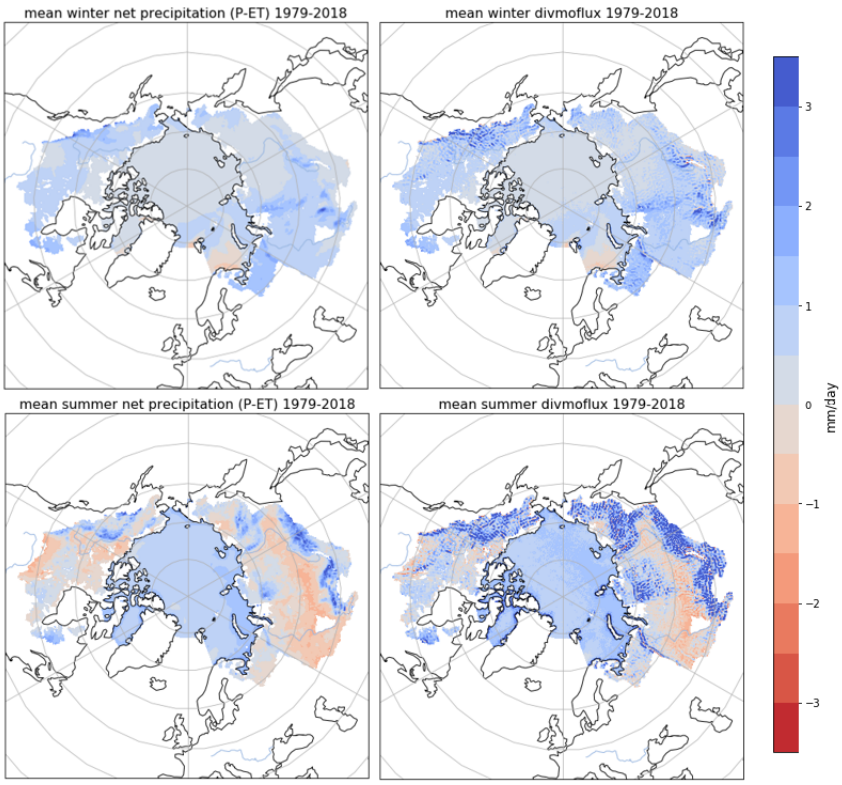

Figure 13: ERA5 winter (D-J-F) and summer (J-J-A) net precipitation (top) and moisture flux divergence (bottom). The mean is calculated over the period 1979-2018, units are mm per day.

domain.

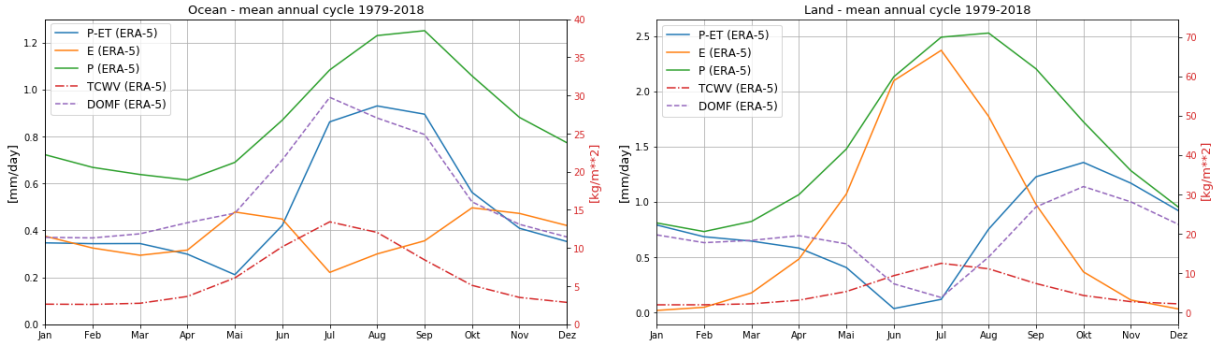

Figure 14: Mean annual cycles of ERA5 precipitation (P [mm/day], green), evaporation (ET [mm/day], orange), net precipitation (P-ET [mm/day], blue), moisture flux divergence (DOMF [mm/day], purple) and total column water vapor (TCWV [kg/m2], red) separately for the ocean and land domain. Means are calculated over the period 1979-2018.

Over the ocean P-ET and respectively moisture flux divergence have their maximum from July to September, the minimum lies in May and in the cold season. The annual cycle of precipitation shows a quite similar distribution, with the difference of a broader summer peak. The evaporation over the ocean domain has it's minimum in July and rises then to a maximum in October. while the melting of sea ice continues through summer and the open water area reaches its maximum in September, the air mass begins to cool and the specific humidity falls resulting in strong water vapour gradients. Similarly there's a small peak of ET in May, coincident with the start of sea ice melt in spring. In early summer, as the air begins to warm again and specific humidity rises, ET starts to sink. The total column water vapour follows the annual cycle of temperature with a minimum in winter and a maximum in summer. Results agree quite well with Serreze et al. (2006), who performed the study with ERA-40 reanalysis.

The main difference when looking at the annual cycle over the land domain is the clear minimum of P-ET and moisture flux divergence in June and July. While precipitation still is largest in summer, it's compensated by a strong evaporation maximum. As mentioned above this maximum develops through the summer warming of the landmasses. The total column water vapour again follows the annual cycle of temperature.

4.2 Interannual Variability and Trends

Figure 15 shows the spatially averaged annual means of net precipitation and moisture flux dievrgence from ERA5 for the period 1979 to 2018. Next to the fluxes overlying the total Arctic area (solid lines), also the individual fluxes over the land domain (dotted lines) and oceanic domain (dashed lines) are displayed. The total fluxes of net precipitation and moisture flux divergence are in relatively good agreement, in the period from 1979 to 1990 they are even practically identical. From 1991 onward moisture flux divergence shows slightly higher values than P-ET. This is equivalent to a rise in total column water vapour (TCWV) from the early 90ies onward, as displayed in figure 16. This rise in TCWV is caused by warming of the atmosphere, as a warmer atmosphere is able to hold more water, and is not present in older versions of ECMWF and NCEP/NCAR reanalysis, but is found in satellite retrievals (see section 2.1.4).

The individual fluxes for ocean and land show bigger differences. While the distribution of maxima and minima between moisture flux divergence and P-E is similar for

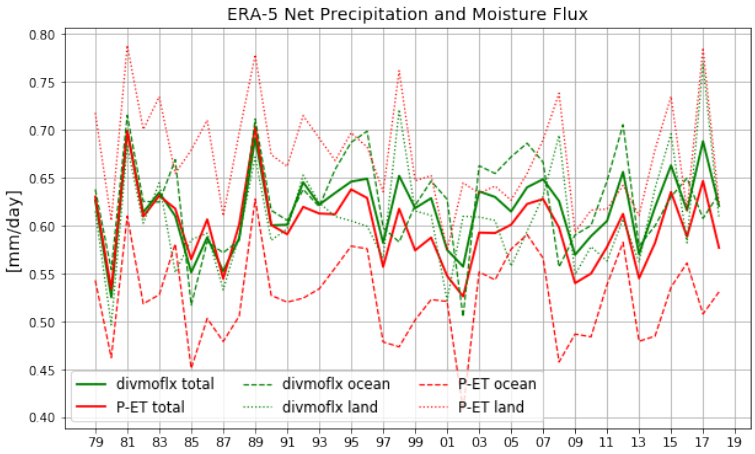

Figure 15: Annual means of ERA5 net precipitation (red) and moisture flux divergence (green). Values over the whole domain (solid lines) and separately for land (dotted lines) and ocean (dashed lines) are shown.

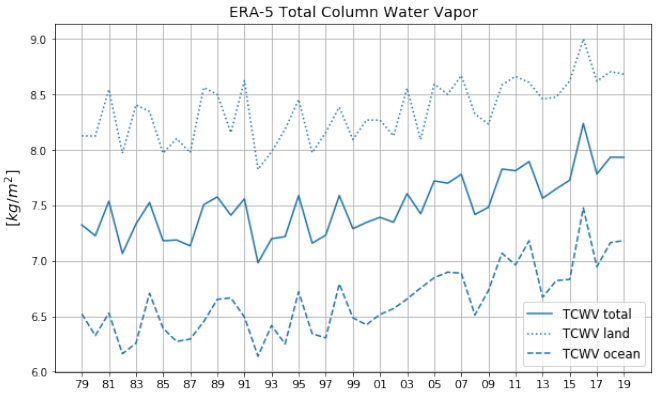

Figure 16: Annual means of ERA5 TCWV for the whole domain (solid line), the land domain (dotted line) and the ocean domain (dashed line) are displayed.

all three domains (land, ocean and total), there are still quite big differences concerning the absolute values for the separated land and ocean domains. Over land the difference between P-ET and moisture flux divergence is biggest at the beginning of the time series, with the fluxes converging towards the more recent years. Over the oceanic domain the difference between the fluxes is quite big throughout the whole period, with moisture flux divergence exceeding net precipitation. Time averages incl. uncertainties calculated as temporal standard deviations and normalized RMSEs are given in table 2. The temporal average of total net precipitation agrees with the average of moisture flux divergence within the calculated standard deviation. The averages for the land

domain are only slightly outside of the standard deviation. The oceanic domain shows the biggest differences with P-E and moisture flux divergence disagreeing by almost 20 percent. The normalized RMSE values confirm that the best agreement is found for the fluxes overlying the whole (land+ocean) Arctic area.

	Net Precipitation	**Moisture Flux Divergence**	**RMSE_norm**
Total	0.60 ± 0.04	0.62 ± 0.04	0.03
Ocean	0.53 ± 0.05	0.63 ± 0.05	0.13
Land	0.67 ± 0.05	0.61 ± 0.05	0.09

Table 2: Time averages of P-ET and moisture flux divergence as well as normalized RMSEs for the total Arctic, the terrestrial and the oceanic domain. Uncertainties are calculated as temporal standard deviations.

The annual cycles in figure 14 confirm the differences of P-ET and moisture flux divergence. Over the ocean moisture flux divergence considerably exceeds P-ET in spring and early summer. In the atmosphere overlying the land domain, P-ET exceeds moisture flux divergence in late summer, autumn and winter, while in spring and early summer moisture flux divergence rises above P-ET. Looking back at figure 13 especially the difference between P-ET and moisture flux divergence over the oceanic domain in summer can be seen, with moisture flux divergence exceeding net precipitation in the eastern part of the ocean.

Figure 17 shows trends of precipitation, evaporation, net precipitation and moisture flux divergence from ERA5 for the period 1979 to 2018. Evaporation exhibits a strong positive trend at Barents and Kara Sea and a slightly weaker one at Chukchi Sea (near Bering Strait). Those evaporation increases are probably caused due to rising sea surface temperatures (SST) and sea ice retreat. Figure 18 shows the trends of SST for the period 1979 to 2018. Nearly the whole Arctic Ocean exhibits positive SST trends, with Barents, Kara and Chukchi Sea exhibiting the strongest changes, matching the positive evaporation trends. The warmer the water gets, the greater gets the evaporation and through more evaporation there's more water available in the atmosphere for precipitation. So similar to SST and evaporation the fields of precipitation also show positive trends in the mentioned areas. However not only increasing evaporation, but also changes in moisture flux divergence and cyclone activity are possible contributors to rising precipitation trends. With evaporation trends exceeding trends in precipita-

tion large parts of the Arctic area, especially Barents Sea, Kara Sea and the Beaufort Sea, show decreasing net precipitation trends and thus a decrease in freshwater delivery to the surface. This is the exact opposite of the results from the studies presented in section 2.1.3, where P shows greater trends than ET resulting in positive P-ET trends. An exception builds the central Arctic Ocean, Greenland and parts of the terrestrial area, where slight positive P-ET trends are present.

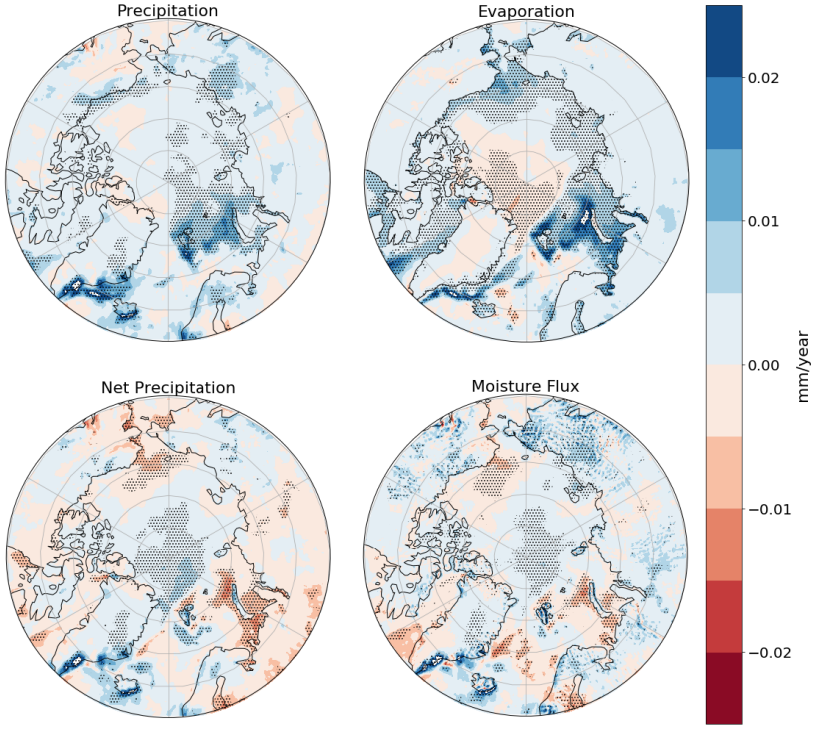

Figure 17: Trends of ERA5 precipitation, evaporation, net precipitation and moisture flux divergence. Dotted areas show significant trends. Trends are calculated for the period 1979-2018, units are mm/year.

Comparing the fields of net precipitation and moisture flux divergence, the biggest differences arise over the terrestrial areas. While net precipitation exhibits predominantly negative values, e.g. over Siberia, divergence of moisture flux tends to increase over most of the terrestrial regions. Those results correspond quite well with figure 15, where the annual means of moisture flux divergence and net precipitation over land converge against each other with P-ET featuring a negative trend and moisture flux divergence exhibiting a positive one.

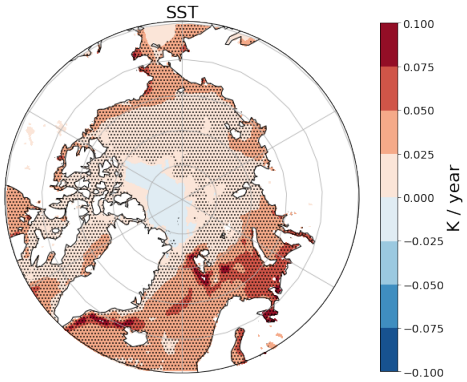

Figure 18: Trends of ERA5 SST for the period 1979-2018. Dotted areas show significant trends. Units are K/year.

4.2.1 Modes of Atmospheric Variability

As described in section 1.3 various large-scale modes of atmospheric variability affect the Arctic region. In this section NAO/AO indices are calculated and the effect of those modes on total precipitation is examined.

The NAO index can be obtained by comparing individual pressure time series between Iceland and the Azores or by using empirical orthogonal function (EOF) analysis. Both methods have their advantages and disadvantages. While station-based indices provide longer time-series than gridded fields, EOF approaches have the benefit of using the entire atmospheric field to extract the modes of variability. Here fields of NAO and AO are obtained through EOF analysis on winter (December-February) mean sea level pressure (MSLP) fields from ERA5. Figure 19 shows the first EOF modes for the Atlantic sector(20-90°N, 80°W-40°E) and for the Northern Hemisphere(20-90°N), showing the structures of NAO and AO.

To examine the hydrological impact of NAO Rogers et al. (2001) compared the NAO/AO indices with P-ET from NCEP/NCAR reanalysis averaged over the northern polar cap (north of 70°). For winter they obtained a correlation of 0.49 between P-ET an NAO and 0.56 between P-ET and AO. For annual P-ET the correlation with NAO was even stronger with 0.69 (0.49 for AO). Figure 20 shows the indices of winter NAO and AO, based on the first principal component of the Atlantic sector MSLP (20-90°N, 80°W-40°E) and the Northern Hemisphere MSLP (20-90°N), as well as the time series of winter (DJF) P-ET north of 65°N from ERA5 reanalyses. Besides small

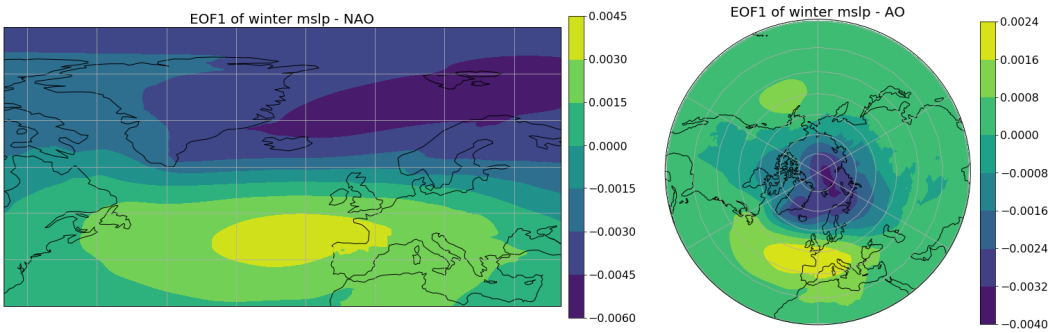

Figure 19: First EOF of winter (Dec-Feb) MSLP over the North Atlantic sector (NAO, calculated over 20-90°N, 80°W-40°E) and over the Northern Hemisphere (AO, calculated over 20-90°N) over the 1979-2019 period, calculated from ERA5 reanalysis.

inconsistencies, the time series structure of AO and NAO are very similar. Looking at the series of P-ET, the connection to NAO/AO can be seen clearly, with maxima and minima being in quite good agreement. Table 3 shows the correlation coefficients

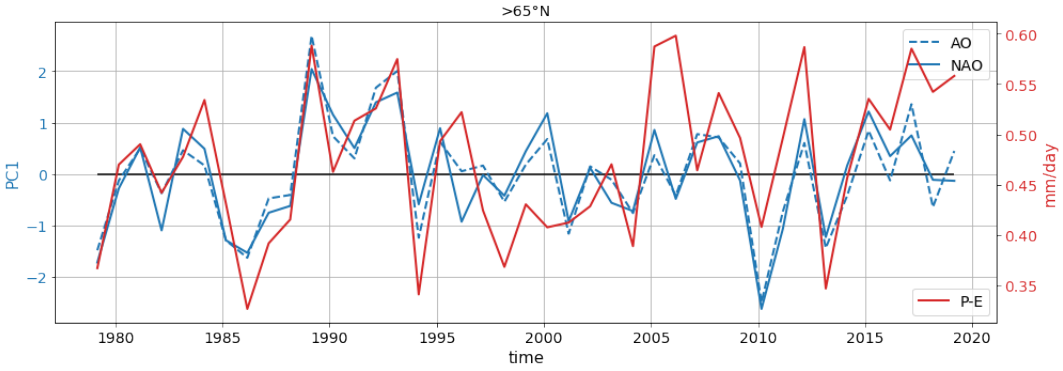

Figure 20: Normalized indices of winter NAO and AO based on the calculation of the first principal components of the Atlantic MSLP and the Northern Hemisphere MSLP and time series of winter P-ET north of 65°N from ERA5 reanalyses.

between the detrended time series of NAO/AO and P-ET north of 60, 65 and 70 °N for winter and annual values. With a value of 0.51 winter correlation between NAO and P-ET north of 70 °N is slightly higher than the value found by Rogers et al. (2001), while AO winter correlations coincide exactly with a value of 0.56. Annual P-ET correlates with NAO(AO) at 0.55 (0.61). In this study the Arctic basin isn't limited to be north of 70 °N as in Rogers et al. (2001), but expands regionally further south. Extending the basin size further south to 65 and 60°N, the correlation coefficients between NAO/AO

and P-ET keep increasing. The hydrological impact of NAO/AO events varies not only

	NAO		AO	
	Annual	Winter	Annual	Winter
>70°N	0.55	0.51	0.61	0.56
>65°N	0.64	0.63	0.70	0.72
>60°N	0.72	0.75	0.76	0.82

Table 3: Annual and winter correlation coefficients between detrended P-ET and detrended NAO/AO north of 60°N, 65°N and 70°N.

from year to year, but also regionally. To identify the regions where precipitation increases/decreases with positive NAO conditions, winter precipitation between low-index NAO and high-index NAO events is examined (figure 21). Therefore total precipitation from ERA5 for the seven weakest NAO events (=highest negative NAO index) between 1979 and 2019 is subtracted from the seven strongest (=highest positive NAO index) ones. Similarly to Xie and Arkin (1996), the major precipitation increases are found in the Norwegian and Greenland Seas. Those increases are presumably due to the changes in Atlantic storm track and cyclone activity mentioned above (Dickson et al., 2000; Serreze et al., 1997). In the central Arctic Ocean the signal is rather low, but

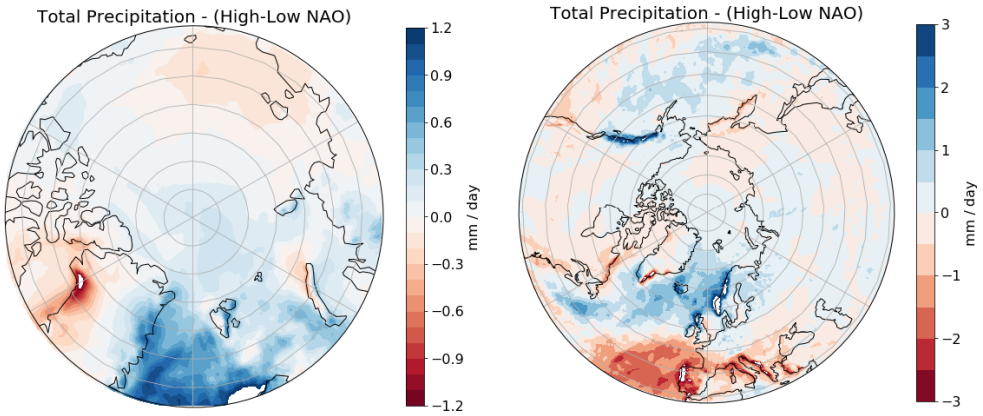

Figure 21: Total precipitation difference from ERA5 reanalysis between high and low NAO events for the central Arctic region and the better part of the Northern Hemisphere. Differences are calculated by subtracting total precipitation for the seven weakest NAO events from the seven strongest ones between 1979 and 2019.

still shows a slight precipitation increase. The regions of Laptev Sea, East Siberian Sea and Chukchi Sea, as well as western Greenland and Baffin Bay show slight precipita-

tion decreases. Expanding the view further south and looking at the entire Northern Hemisphere, precipitation increases associated with NAO are also found on the west coast of North America and strong precipitation decreases occur in the vicinity of the Azores High and the Mediterranean Sea.

4.3 Land

Next to P-ET a key factor for the hydrological budget is runoff R. For the terrestrial domain runoff comprises a freshwater sink, while for the ocean delivery of freshwater through runoff builds an important freshwater source.

Figure 22 shows the mean annual cycles of the hydrological land components from ERA5 for the four biggest terrestrial drainage basins Yenisei, Ob, Lena and Mackenzie over the period 1979-2018. Next to P-ET and runoff (R) it's also important to look at the snow components snowfall (SF) and snowmelt (SMLT) in order to consider the seasonal snow storage. Additionally observed runoff from ArcticGRO is shown.

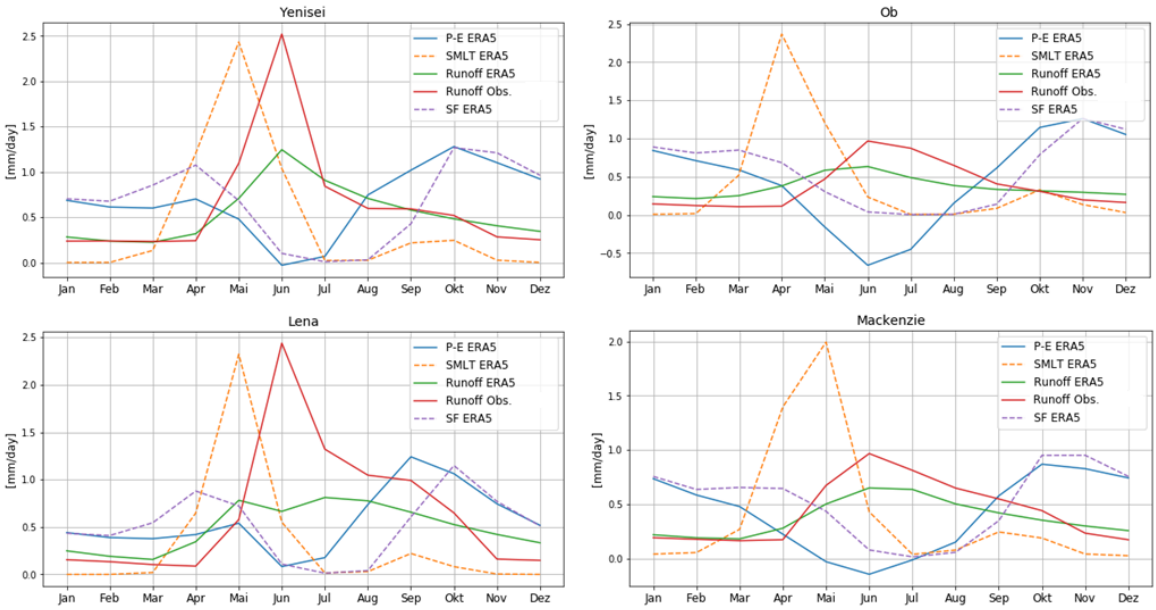

Figure 22: Mean annual cycles of the hydrological land components P-ET, SF, SMLT and R from ERA5, as well as observed runoff from ArcticGRO.

The cycle of P-ET for the individual basins is quite similar to P-ET over the whole terrestrial domain (see fig. 14), with maxima in autumn and minima in summer. The snowfall curve shows the fraction of total precipitation that falls as snow. Snowfall rises in autumn and has it's maximum in October. With decreasing total precipitation in winter, as terrestrial cyclone activity and convection have their minimum, snowfall declines somewhat, but still stays quite high through winter. With precipitation rising in spring, snowfall has a slight second maximum before falling to it's minimum in late spring/early summer. Snowmelt on the other side only has a small peak in autumn corresponding to the start of snowfall and then, with temperatures falling, stays low

until spring. With temperatures rising in spring, snowmelt rises promptly to a strong maximum in May (April for the Ob basin). However the maximum in runoff occurs a little bit later in June, as meltwater needs some time to gather in streams and rivers and to run through the basin into it's discharge point to the ocean or the gauging point. While observed runoff from ArcticGRO and runoff from ERA-5 show similar cycles with the highest values in spring and the beginning of summer and minima in winter, there's a big difference concerning the height of the peaks. Especially at the Yenisei and Lena basins the maxima from observations are way more pronounced than their ERA5 reanalysis equivalents.

4.3.1 Runoff - Interannual Trends

The time series of observed runoff from the ArcticGRO project for the four major Arctic river basins Ob, Yenisei, Lena and Mackenzie is shown in figure 23. Yenisei and Lena deliver the biggest amount of freshwater to the ocean with a mean annual discharge of 602 and 568 km^3 per year. Ob delivers about 410 km^3 of freshwater per year and Mackenzie about 290 km^3/yr. All four basins together are responsible for about 68 percent of the total Arctic river runoff (Serreze and Barry, 2014), with the total discharge from the Eurasian river basins being generally about three to four times greater than discharge from the North American basins (Holmes et al., 2018). All four basins show positive trends, with Lena featuring the steepest runoff increases.

In the following section observed runoff is compared with runoff from reanalysis for Yenisei, Ob, Lena and Mackenzie separately. Next to direct runoff from ERA5, also Runoff from the GloFAS 2.1 project, that combines the ERA5 land surface model (HTESSEL) with a hydrological model (LISFLOOD), is considered. Furthermore runoff from ERA5-Land, the offline (surface downscaled) equivalent of ERA5, and the corresponding offline GloFAS 2.3 project, that takes ERA5-Land as input, are viewed. Above all the direct runoff can be also compared with indirectly calculated runoff. Considering longer time scales the left side of equation 9 can be dropped. So averaged over each catchment, runoff should be equal to net precipitation. So additionally to direct runoff the annual means of P-E from ERA5 are also shown.

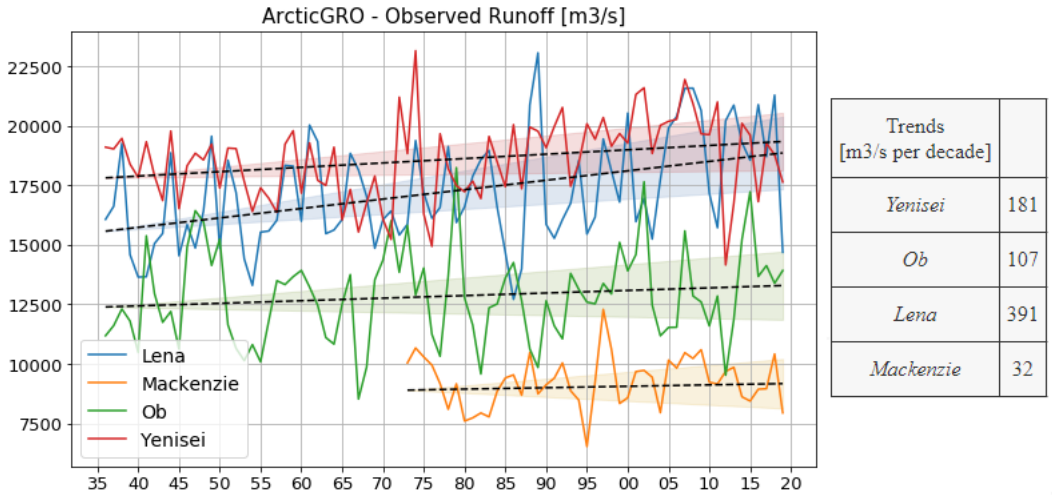

Trends [m3/s per decade]	
Yenisei	181
Ob	107
Lena	391
Mackenzie	32

Figure 23: Observed long term trends in annual runoff for the four major drainage basins from ArcticGRO. Shaded areas mark the 95% confidence intervals of the trends and the table provides trend values in m^3/s per decade.

Yenisei: Figure 24 shows the various runoff variables for the Yenisei catchment. The annual means of the observed runoff from the ArcticGRO-Project and runoff from ERA5 reanalysis exhibit great differences. Up until 1990 the values are quite similar, but afterwards ERA-5 runoff starts to decline rapidly. Especially at the beginnings of the nineties and the start of the 21st century ERA5 runoff shows big downward jumps, leading to significant differences in the past three decades. Runoff from GloFAS 2.1 shows a similar progress as ERA5 runoff, which is expected as GloFAS 2.1 takes ERA5 as input and the time delay through river routing is averaged out through calculation of whole annual means (Zsoter et al., 2020).

In contrast ERA5-Land tends to slightly overestimate runoff up to the late nineties and afterwards is in quite good agreement with runoff observations. The offline experiment GloFAS 2.3, which uses ERA5 Land as input, is only available from 1999 to present. In this period runoff values are a little bit lower than the ones from ERA-5 Land, but generally don't differ to much from observed discharge and show way better results than ERA5 and GloFAS 2.1. With atmospheric forcing and the land surface model being virtually the same in ERA5 and ERA5-Land, the differences in runoff are probably due to the absent coupling and land data assimilation, that has impacts on snow and soil moisture, and the higher resolution and lapse-rate correction in ERA5-Land (Zsoter et al., 2020). This issue will be examined closer in the next chapter.

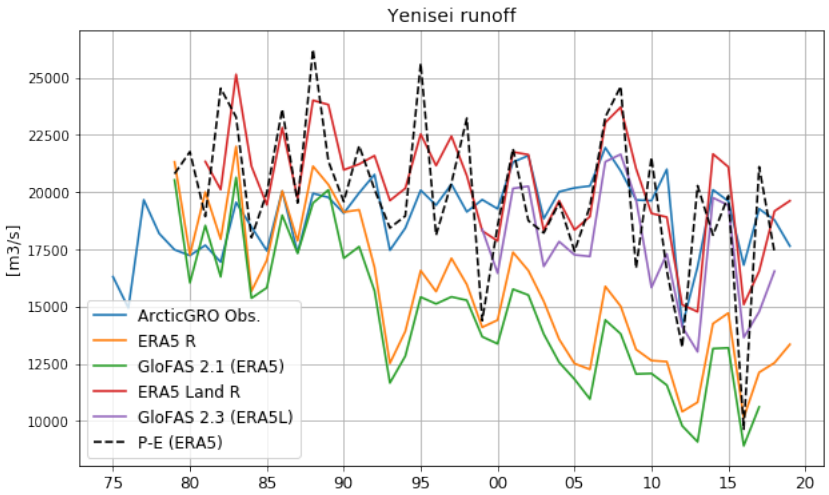

Figure 24: Observed runoff from the ArcticGRO project, runoff from ERA5, ERA5-Land, GloFAS 2.1 and GloFAS 2.3 as well as indirectly calculated runoff through P-ET for the Yenisei catchment area.

The indirectly calculated runoff from ERA5, namely net precipitation, shows significantly better results than direct runoff from ERA5 and GloFAS 2.1, and is quite similar to ERA5-Land and GloFAS 2.3 with more distinct peaks and minima.

Ob: For the Ob basin, direct runoff from ERA5 is in better agreement with observed runoff, than for the Yenisei catchment. Again it shows a negative trend, however it's way less pronounced than the trend at the Yenisei basin. GloFAS 2.1 shows a similar progress like ERA5, but a clear shift to lower discharge values and hence underestimates runoff by about 40% in comparison to ERA5. ERA5-Land again tends to overestimate runoff, especially in the first two decades and features a slight negative trend, comparable to ERA5. Runoff from the corresponding GloFAS 2.3 shows, as expected, a similar progress like ERA5-Land, but, just as GloFAS 2.1, clearly underestimates the actual runoff values. The indirectly calculated runoff (P-ET) again is quite similar to ERA5-Land with more distinct peaks.

Lena: For the Lena basin, again both GloFAS 2.1 and GloFAS 2.3 show similar progresses to ERA5 and ERA5-Land, but strongly underestimate actual runoff with values only about half as big as the observations. Up until 1990 runoff from ERA5 is in good accordance with the observed values, but afterwards the time series start

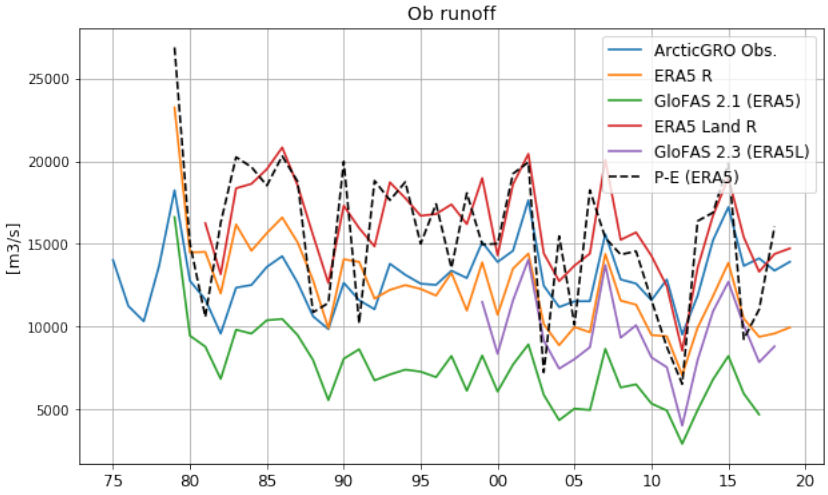

Figure 25: Observed runoff from the ArcticGRO project, runoff from ERA5, ERA5-Land, GloFAS 2.1 and GloFAS 2.3 as well as indirectly calculated runoff through P-ET for the Ob catchment area.

to diverge and with a strong negative trend of ERA5 the difference becomes huge at the end of the considered period. ERA5-Land runoff and P-ET from ERA5 once again show quite similar results and agree with the observation up until the late nineties, but afterwards, as observed runoff tends to increase, the difference rises to about 15 to 25 percent in the past decade.

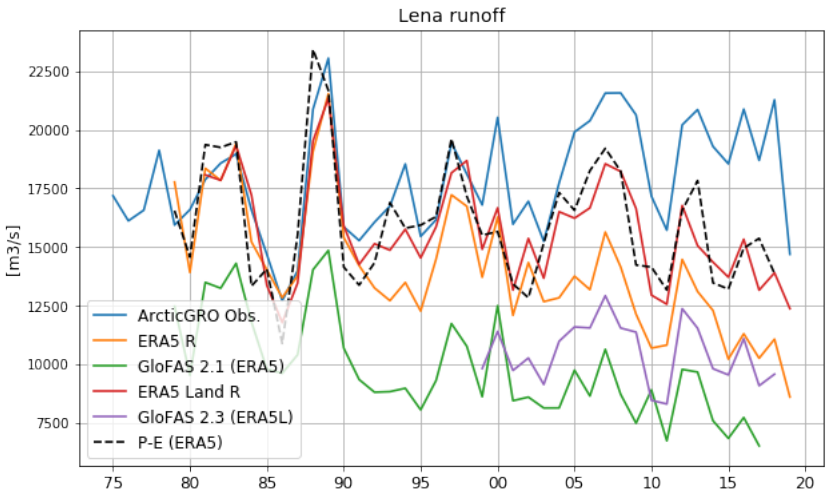

Figure 26: Observed runoff from the ArcticGRO project, runoff from ERA5, ERA5-Land, GloFAS 2.1 and GloFAS 2.3 as well as indirectly calculated runoff through P-ET for the Lena catchment area.

Mackenzie: Figure 27 shows the various runoff variables for the Mackenzie catchment. Once again runoff from GloFAS 2.1 and ERA5 show similar progresses, with GloFAS 2.1 strongly underestimating the actual runoff and only accounting for about 40 to 60 percent of the observed runoff values. Up to the start of the 21st century runoff from ERA5 fits quite well to observed runoff, but afterwards, due to a strong negative trend in ERA5 and a slightly positive trend in the observations, observed runoff and ERA5 runoff start to diverge and exhibit great differences in the past decade. Values from ERA5-Land show a clear improvement and accord well with the observations, while runoff values from GloFAS 2.3 again tend to clearly underestimate actual runoff. The indirectly calculated runoff through P-ET from ERA5 exhibits significantly stronger maxima and minima than observed runoff, but generally fits quite well.

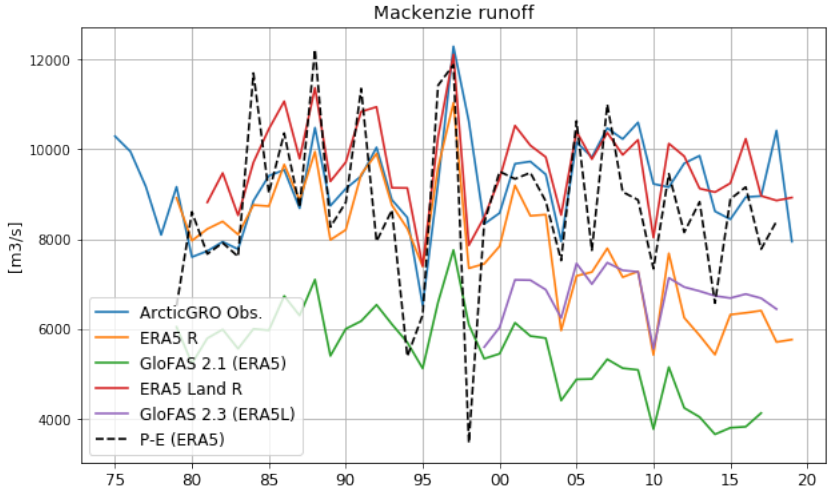

Figure 27: Observed runoff from the ArcticGRO project, runoff from ERA5, ERA5-Land, GloFAS 2.1 and GloFAS 2.3 as well as indirectly calculated runoff through P-ET for the Mackenzie catchment area.

In order to compare the various runoff variables quantitatively, table 4 shows timely means of all runoff parameters, as well as the calculated Root Mean Square Errors (RMSEs) and correlation coefficients r in comparison to the observed runoff. Values from GloFAS 2.3 have to be viewed with caution, as they are calculated over a shorter period (1999-2018) than the other parameters and hence are disregarded in the following evaluation. Generally the worst results are obtained through GloFAS 2.1, with it tending to clearly underestimate the actual runoff values. Looking at the perennial means, at Yenisei, Mackenzie and Lena indirectly calculated runoff (P-ET) fits best to

the observed values, while for Ob direct runoff from ERA5 provides the best results. The cross correlation coefficients r and the RMSEs confirm the conclusion from figures 24 -27 with ERA5-Land runoff and ERA5 P-ET agreeing most with the observations.

	Obs.	**ERA5 R**			**GloFAS 2.1**			**ERA5 P-ET**		
	Mean	*Mean*	*r*	*RMSE*	*Mean*	*r*	*RMSE*	*Mean*	*r*	*RMSE*
Yeni.	19.1	15.63	0.19	4.72	14.65	0.16	5.54	19.87	0.35	3.14
Ob	13.0	12.38	0.54	2.48	7.38	0.56	5.97	15.47	0.52	4.41
Lena	18.0	14.07	0.29	4.95	9.83	0.24	8.59	16.02	0.58	3.06
Mack.	9.19	7.83	0.26	2.01	5.47	0.32	3.90	8.72	0.37	1.75
	Obs.	**ERA5-L R**			**GloFAS 2.3**					
	Mean	*Mean*	*r*	*RMSE*	*Mean*	*r*	*RMSE*			
Yeni.	19.1	20.29	0.59	3.05	17.57	0.80	2.43			
Ob	13.0	16.06	0.68	4.46	9.50	0.89	4.07			
Lena	18.0	15.69	0.66	4.07	10.50	0.73	8.62			
Mack.	9.19	9.64	0.64	1.48	6.77	0.65	2.71			

Table 4: Means of the various runoff parameters as well as RMSEs and correlation coefficients r, calculated from annual means over the period 1979-2018. Units are $m^3/s * 10^{-3}$.

Figure 28 shows runoff from ERA5 and ERA5-Land calculated over all 64 catchments defined in figure 2. Considering the whole terrestrial region, runoff from ERA5-Land outstrips ERA5 runoff by more than 30%. Both datasets show negative trends, with the decrease in ERA5 happening almost twice as fast as in ERA5-Land.

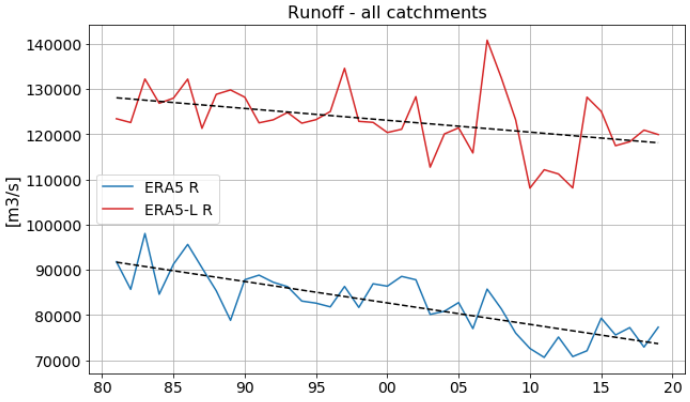

	ERA5 R	ERA5-L R
$\mu[\mathrm{m}^3 s^{-1}]$	82702	123120
$\sigma[\mathrm{m}^3 s^{-1}]$	6664	6930
Trend $[m^3 s^{-1} yr{-}1]$	-474	-262

Figure 28: Runoff from ERA5 and ERA5-Land calculated over all 64 catchments.

4.3.2 Runoff - Observation vs. ERA5

Seasonal Changes

To assess the differences between observed runoff and runoff from ERA5 and ERA5-

Land more precisely, figure 29 shows runoff trends from ERA5, ERA5-Land and observations for the Yenisei, Ob, Lena and Mackenzie basin for all seasons (DJF-winter, MAM-spring, JJA-summer and SON-autumn) individually. As expected, observations as well as ERA5 and ERA5-Land agree that annual discharge is dominated by summer runoff, followed by runoff from autumn and spring, and winter discharge being the weakest one. Noticeable is the high ERA5-Land spring runoff at the Ob basin, which explains the general annual runoff overestimation by ERA5-Land at the Ob catchment (figure 25).

While the annual values from observations exhibit slightly positive trends at all four basins, not all seasons contribute equally to those increases. Autumn, winter and spring runoff have increased over the past decades and show positive trends at all catchments, while summer runoff features at Yenisei and Mackenzie strong negative trends of up to 20%. Lena and Ob river feature no significant trend during summer time and summer values at Lena basin are almost twice as high as the ones from ERA5 and ERA5-Land. In contrast, annual discharge from ERA5 shows clear decreases at all four basins and those trends are caused through contribution from all seasons. Again summer values feature the strongest changes, but also the other seasons show negative trends. Runoff from ERA5-Land similarly shows predominantly negative, but weaker trends.

To asses this quantitatively table 5 shows the calculated linear trends for the period 1981-2019 at all basins for all seasons in m^3 per year. Positive values characterize runoff increases and negative values decreases. As expected runoff from ERA5 shows merely and ERA5-Land predominantly negative trends, while observed runoff, except for summer, exhibits positive trends.

As not only natural causes like e.g. permafrost degradation or enhanced precipitation affect changes in discharge behaviour, but also human activities, like river regulation systems, play an important role, it's not easy to separate real natural changes from man made changes. Rising temperatures cause thawing and snowmelt processes to start earlier, leading to a runoff shift from summer to spring, hence the increase in spring runoff and decrease in summer runoff. Furthermore the melt of permafrost and

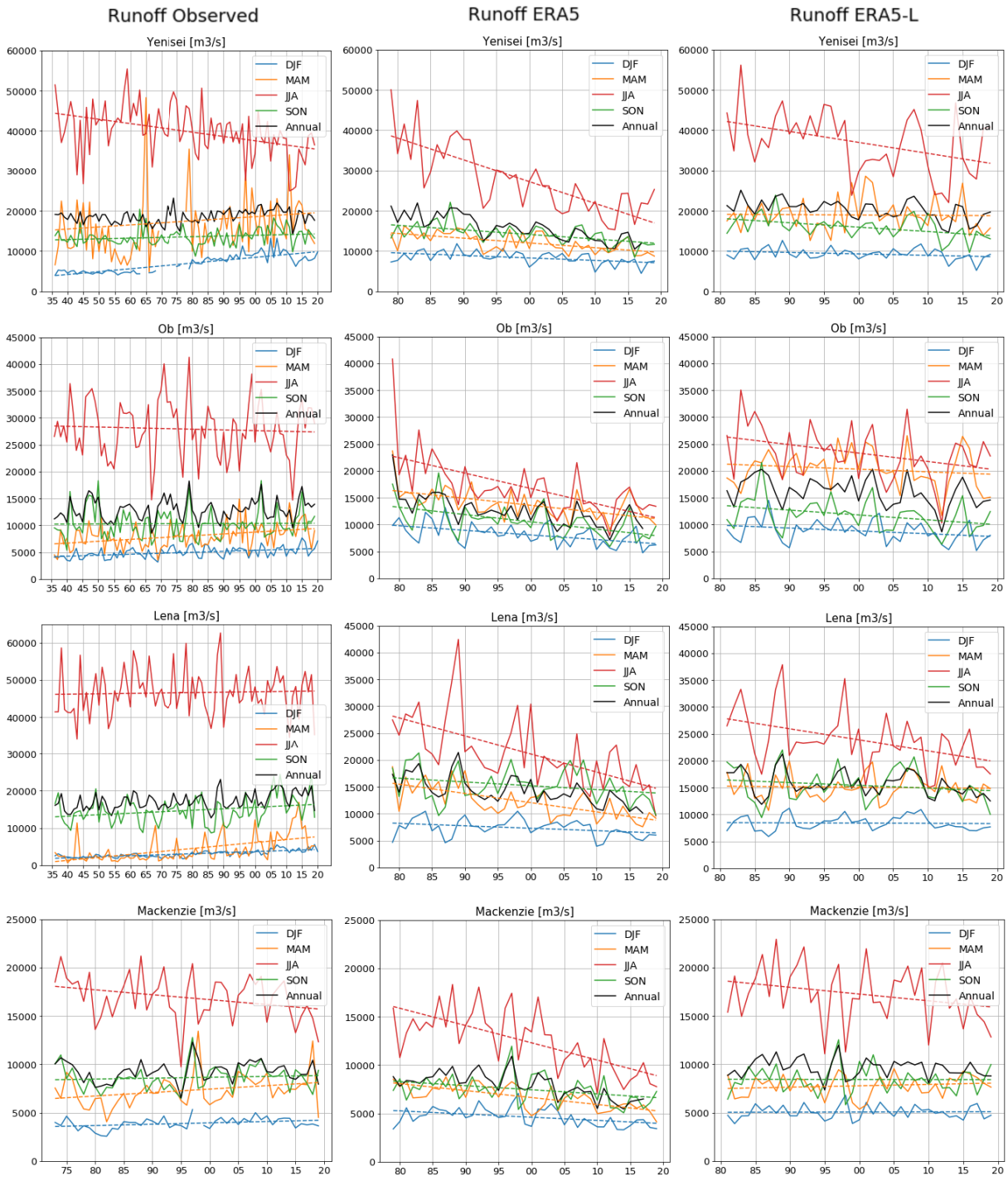

Figure 29: Runoff trends for Yenisei, Ob, Lena and Mackenzie River from ERA5, ERA5-Land and observations for winter (DJF-December, January, February), spring (MAM-March, April, May), summer (JJA-June,July,August) and autumn (SON-September, October, November). Units are m^3/s. Note the different time scales for observations (1936-2019 and 1973-2019) and reanalyses (1981-2019).

precipitation more frequently falling as rain instead of snow could likewise contri-

Trends 1981-2019 [m3/yr]	**Annual**			**Winter (DJF)**			**Spring (MAM)**			**Summer (JJA)**			**Autumn (SON)**		
	Obs.	*E5*	*E5-L*	*Obs.*	*E5*	*E5-L*	*Obs.*	*E5*	*E5-L*	*Obs.*	*E5*	*E5-L*	*Obs.*	*E5*	*E5-L*
Yenisei	16	-210	-107	36	-62	-36	34	-118	-8	-185	-540	-272	73	-114	-109
Ob	25	-159	-88	9	-86	-53	60	-131	-49	2	-286	-157	25	-136	-90
Lena	76	-158	-68	37	-45	-5	147	-172	-10	-11	-336	-206	132	-71	-52
Mack.	21	-82	-14	20	-33	1	54	-72	14	-31	-179	-70	26	-43	-1

Table 5: Seasonal and annual runoff trends for Yenisei, Ob, Lena and Mackenzie from ERA5, ERA5-Land and observations for the period 1979-2019. Units are m^3/yr.

bute to rising runoff trends in autumn, winter and spring. However, as mentioned in section 2.1.6, also dam regulation systems could play a part, as they redirect runoff from the high-flow month in summer to low-flow winter month.

Surface and Subsurface Runoff

Runoff, as defined in ERA5, builds the sum of surface and subsurface runoff. To identify where the differences between ERA5 and ERA5-Land runoff come from, figure 30 shows annual means of surface and subsurface runoff from ERA5 (solid lines) and ERA5-Land (dashed lines) for the four major catchments individually. According to Zsoter et al. (2020) globally ERA5-Land produces slightly more runoff than ERA5, even though surface runoff exceeds in ERA5. This is due to a much higher global subsurface runoff in ERA5-Land. Considering the Arctic region, at the three major catchments (Ob, Yenisei and Lena) ERA5-Land exceeds ERA5 at subsurface runoff as well as surface runoff, hence both variables contribute to the lower total runoff values in ERA5. At the Mackenzie basin surface runoff seems quite balanced, thus subsurface runoff is responsible for lower values and the negative trend in ERA5 total runoff.

Snow Assimilation

As mentioned above, a possible reason for those negative trends in ERA5 runoff lies in the data assimilation system and its removal of soil moisture. Zsoter et al.(2020) assess the GloFAS 2.1 river discharge reanalysis as well as ERA5 and ERA5-Land runoff and compare them with available river discharge observations. Similarly to the figures above, Zsoter et al. (2020) find river discharge decreases in GloFAS-ERA5 for several major world rivers, that are not supported by observations. They find trends in tropical and subtropical areas being driven by changes in precipitation, while changes in snowmelt have a very strong influence on river discharge trends in the northern

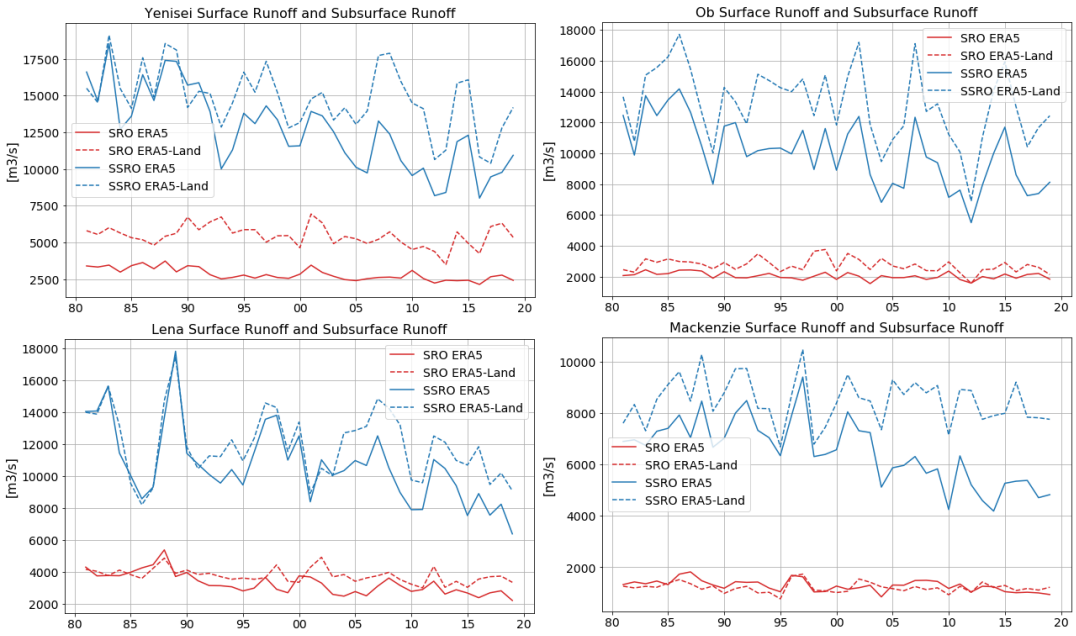

Figure 30: Surface and subsurface runoff from ERA5 and ERA5-Land for the Yenisei, Ob, Lena and Mackenzie basins.

latitudes. Thus the runoff decreases in the northern latitudes are likely linked to snow assimilation and other snowmelt-producing processes. (Zsoter et al., 2020)

Therefore figure 31 shows ERA5 snowfall, snowmelt and the sum of snowmelt and snow evaporation for the Yenisei, Ob, Lena and Mackenzie basins as well as the corresponding parameters from ERA5-Land. For longer time scales snowfall and the sum of snowmelt and snow evaporation should be in balance. As seen in figure 31, that's clearly not the case with ERA5 reanalysis. Especially for Yenisei and Lena the difference between snow input and snow output is significantly big in the past two decades, with a pronounced negative trend and clear discontinuities around 1990 and 2004. At Ob basin a discontinuity is only found around 1990 and at Mackenzie there's a slight jump around 2004. Looking back at the runoff comparison in figures 24 to 27, the corresponding runoff parameters from ERA5 and GloFAS 2.1 exhibit similar discontinuities. In contrast snow input and snow output are in balance for ERA5-Land, as snowmelt from ERA5-Land does not exhibit those pronounced downward shifts around 1990 and 2004. Zsoter et al. (2020) find similar results. Hence with atmospheric forcing and the land surface model being virtually the same in ERA5 and ERA5-Land, the differences in runoff are probably due to the absent coupling and land data assimilation, that has impacts on snow and soil moisture. The snow assimilation system, that is not present

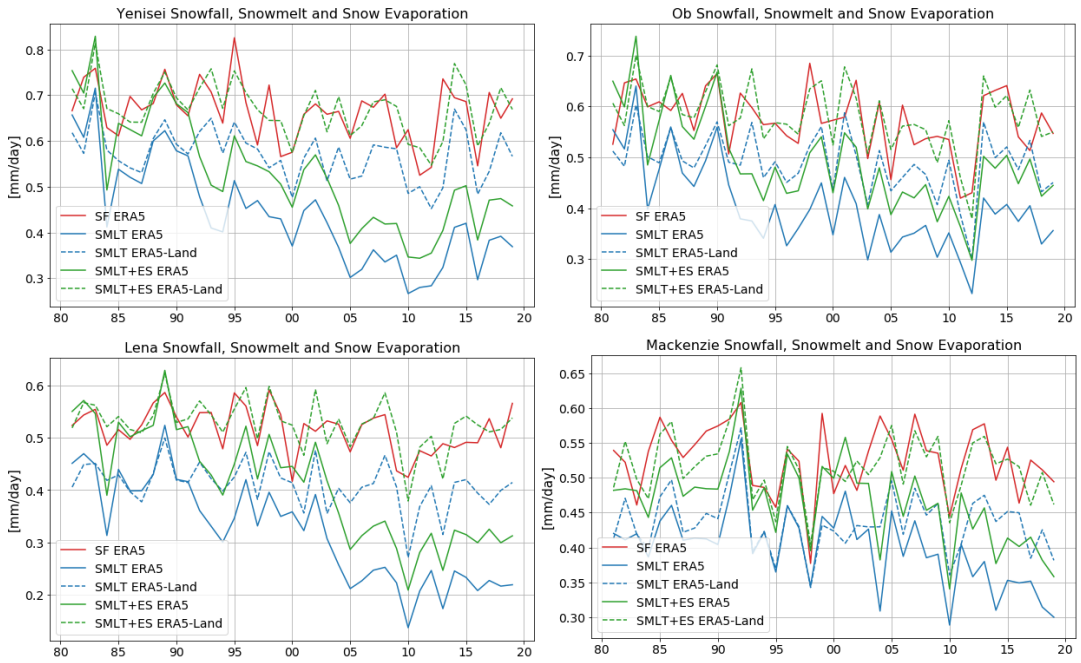

Figure 31: Annual means of ERA5 snowfall (SF, red), ERA5 and ERA5-Land (dashed) snowmelt (SMLT, blue) and ERA5 and ERA5-Land (dashed) snowmelt + snow evaporation (SMLT+ES, green) for the four major Arctic basins Yenisei, Ob, Lena and Mackenzie. Units are mm per day.

in ERA5-Land, has a tendency to remove water from the hydrological cycle due to the snow scheme in HTESSEL and is believed to be, at least partially, responsible for those negative trends (Zsoter et al., 2019; Zsoter et al., 2020). The discontinuity in 2004 was traced back to a change in operational snow analysis, through the introduction of the 24-km Interactive Multi-Sensor Snow and Ice Mapping System (IMS) snow cover information to the snow assimilation system in 2004 (Zsoter et al. 2020). Dutra et al. (2012) assessed and evaluated snow schemes in the HTESSEL and found them to melt snow too slowly. Hence, in combination with IMS snow cover data, the assimilation could remove excess snow that was not melted by the model (in observation-sparse areas) and lead to the documented negative shift in snowmelt. (Zsoter et al., 2020)

Figure 32 shows a Hovmöller diagram for the meridional means of the ERA5 monthly snowmelt anomaly for the region north of 50°N in mm per day. Red values represent negative snowmelt anomalies and blue values positive ones. Again the clear discontinuity around 2004 can be seen, with snowmelt generally being higher before 2004, and lower after the discontinuity. Especially the area around Siberia, but also coastal

regions show prominent changes.

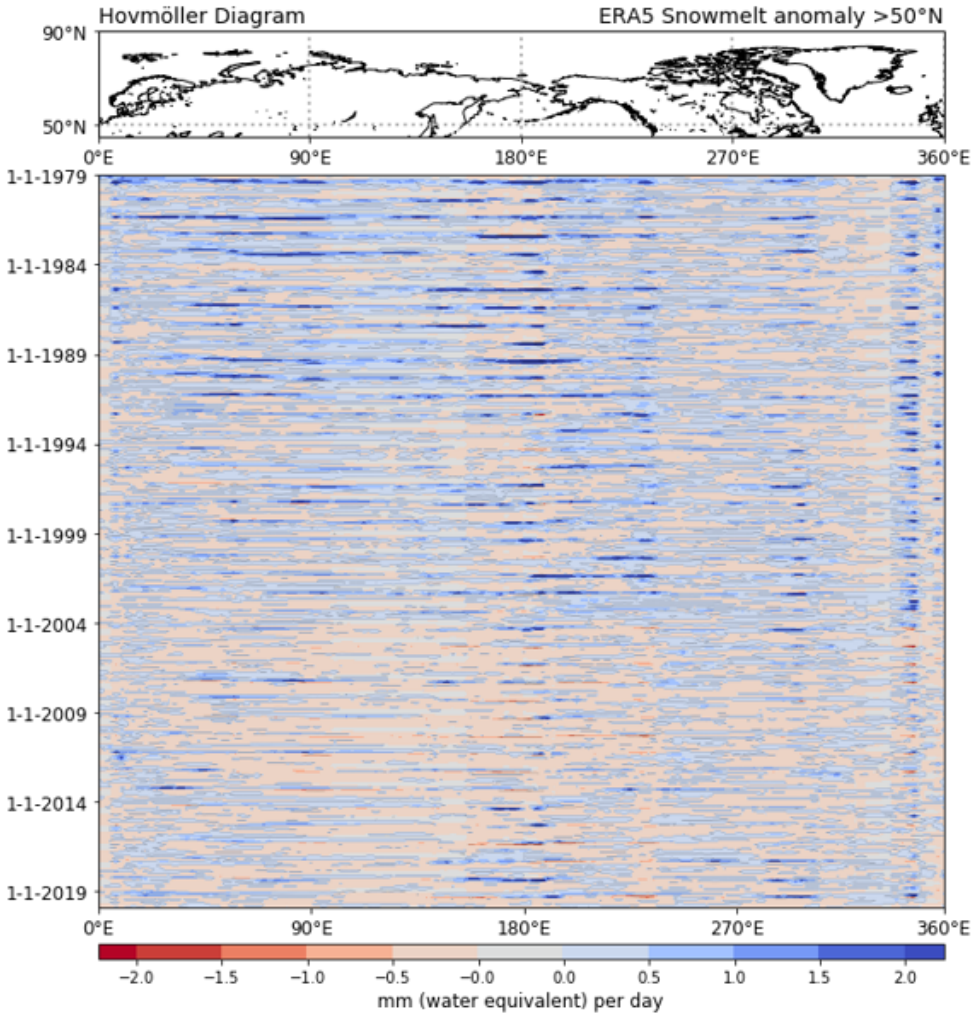

Figure 32: Hovmöller diagram of ERA5 monthly snowmelt anomaly. The y-axis is the time axis with monthly means from January 1979 to December 2019 and the x-axis shows longitudinal degrees. The top plot shows the considered area. Units are mm/day

To get a better understanding about the spatial distribution, figure 33 shows the climatological differences of snowfall, snowmelt and their sum, calculated as difference between 2004-2019 and 1979-2004. Snowmelt shows clear trends, especially at mountainous regions like the Siberian Plateau, the Ural Mountains and the Rocky Mountains, but also coastal areas and Iceland exhibit clear trends. In contrast to snowmelt, snowfall seems far more stable, showing hardly any trends. Subsequently the difference between snowfall and snowmelt is dominated by the changes in snowmelt and shows negative trends, especially at mountainous regions.

Zsoter et al. (2020) furthermore analyse ERA5 and ERA5-Land trends after remo-

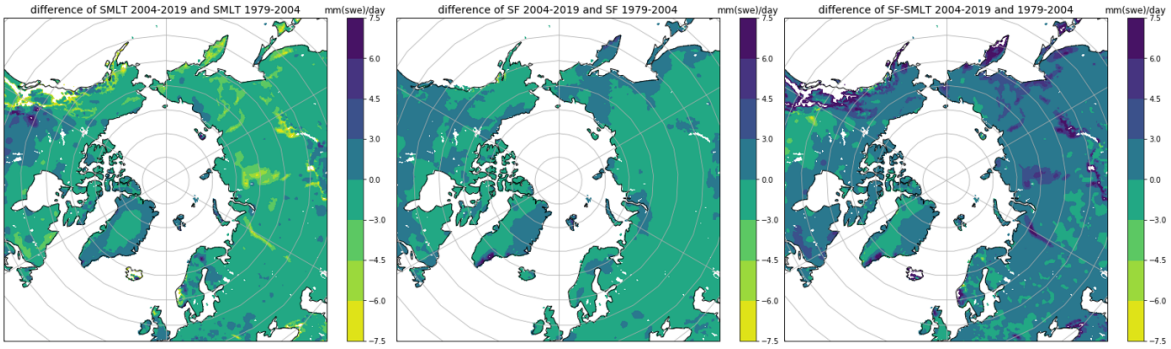

Figure 33: Climatological differences of snowfall, snowmelt and their sum between 2004-2019 and 1979-2004. Units are mm/day.

ving the discontinuity of the IMS satellite snow cover from the time series and find that snow assimilation likely also contributes to negative snowmelt trends before the introduction of IMS in 2004. This is in accordance with the results presented here, as figure 31 shows clear differences between ERA5 and ERA5-Land runoff before 2004, mainly due to a discontinuity around 1990. Also the higher resolution and lapse-rate correction in ERA5-Land might play a part.

Additionally Zsoter et al. (2020) indicate that not only unrealistic trends in the ERA5 forcing, but also deficits in GloFAS directly, like the insufficient handling of human influences, e.g. river regulation, might impact the river discharge trends.

4.3.3 Water storage

The soil is divided into four layers in ECMWFs HTESSEL (see section 3.1.1.) and ERA5 volumetric soil water content (SWCV) is available for all four layers individually. Here the focus lies on layer 1, the upper 7cm of soil that directly impact the atmosphere through evaporation, and the combination of layers 1-3, the upper 100 cm of soil which represent slower processes but are directly linked to the atmosphere through vegetation roots (Zsoter et al., 2020). Figure 34 shows SWCV from ERA5 and ERA5-Land for Yenisei, Ob, Lena and Mackenzie basin. At all four basins the top 7cm of soil have a higher volumetric soil water content than the layers beneath. That was expected as the top layer is in direct contact with water supplying processes like precipitation and snowmelt. At the Yenisei, Ob and Mackenzie basin SWVC from ERA5-Land exceeds the values from ERA5, while at Lena basin ERA5 is in excess of ERA5-Land. Especially

Lena and Yenisei feature a strong decrease in soil moisture, in the top layer as well as in the deeper soil layers, over the past decade. This decrease could be linked to increasing temperatures, but also permafrost melting could play a part, as with active layer thickening moisture is able to soak into deeper soil layers leading to a dryer surface soil.

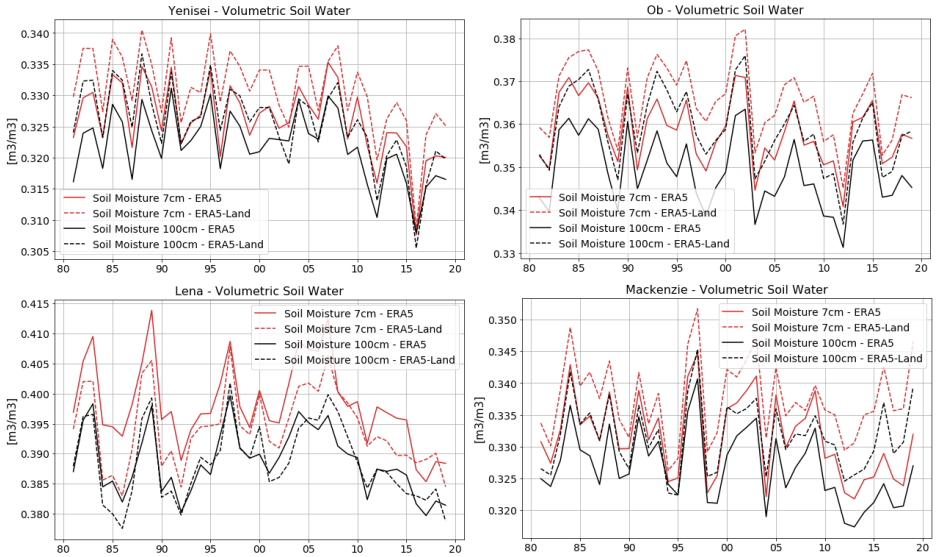

Figure 34: ERA5 and ERA5-Land volumetric soil water content for layer one (upper 7cm) and layers 1-3 (upper 100cm) at the Ob, Yenisei, Lena and Mackenzie basin.

Figure 35 shows the mean annual soil moisture cycles for the four soil layers (0-7cm, 7-20cm, 20-100cm and 100-289cm) from ERA5 and ERA5-Land. Generally seasonal variations are highest in the surface layers and become weaker with depth. Soil moisture in the top two layers peaks in spring (April for Ob and Mai for Yenisei, Lena and Mackenzie), has it's minimum in summer when evaporation is highest and rises again to a secondary maximum in autumn. Through winter soil moisture decreases, as water is also stored above the soil as snow and rises again in spring through snowmelt and increasing precipitation. The third layer (20-100cm) shows a similar, but weaker progress as the layers above, however the spring peak is displaced by one month. Water in the bottom layer exhibits only slight seasonal variations and peaks in summer, when the other layers have their soil water minimum.

4.4 Ocean

4.4.1 Volume fluxes

Figure 36 shows time series of monthly volume fluxes at the four major gateways and the Arctic net volume flux for observations from ArcGate and reanalysis from ORAS5, where the fluxes are calculated directly out of the ocean currents in ORAS5. The considered period is rather short, as ArcGate data is only available from October 2004 to May 2010. The net volume flux is calculated by taking the sum over all straits. Negative values indicate a flux into the Arctic Ocean and positive values fluxes out of the Arctic Ocean. Figure 36 confirms that both Bering Strait and Barents Sea Opening (BSO) transport volume into the Arctic Ocean. However while the inflow through Bering Strait consists of low salinity waters and hence builds a freshwater source, the inflow through BSO has a relatively high salinity and therefore counts as freshwater sink. Davis and Fram Strait deliver volume out of the Arctic, partly as freshwater and partly as saline water. The volume fluxes of the individual straits are quite big and partially reach a couple of Sverdrups (1Sv = $10^6 m^3/s$). The net volume flux however is much lower and reaches values around 140 mSv and should be equal to the total freshwater flux passing through the Arctic gateways. Apart from small exceptions the net flux is generally positive, hence overall the Arctic Ocean loses freshwater through

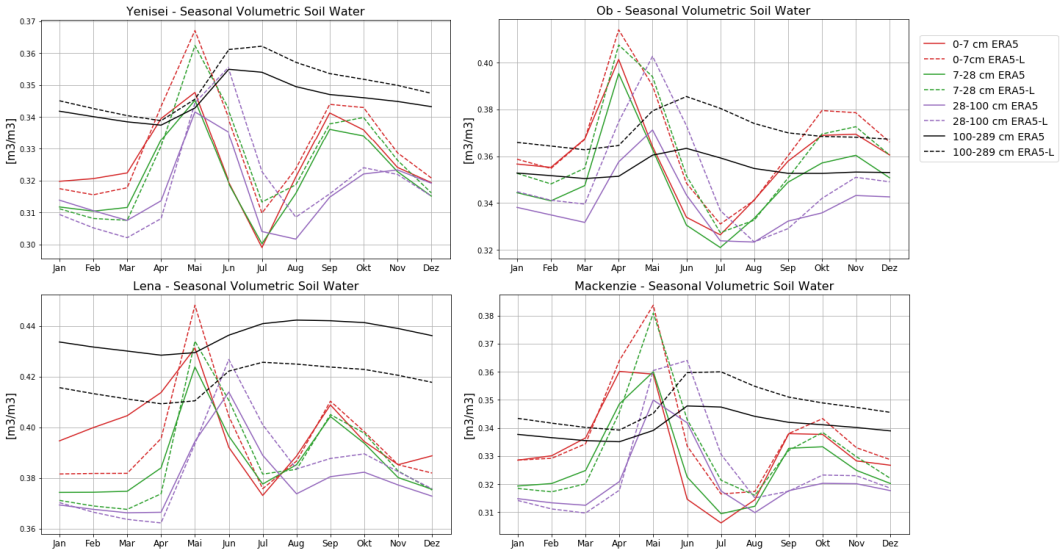

Figure 35: ERA5 and ERA5-Land seasonal volumetric soil water content for all four soil layers at the Ob, Yenisei, Lena and Mackenzie basin.

the gateways. Comparing the observed fluxes from ArcGate with Oras5 reanalysis, the individual fluxes exhibit quite big differences.

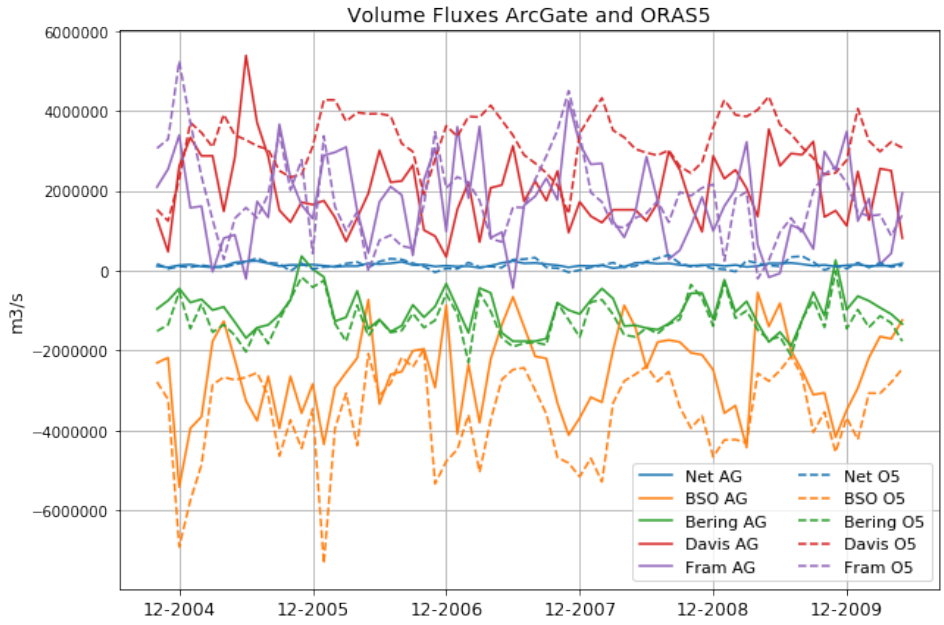

Figure 36: Volume fluxes through the Arctic gateways as well as the total net flux derived from observations (ArcGate) and from Oras5.

Table 6 shows the mean volume transports and the calculated RMSEs between ArcGate and ORAS5 at the individual straits as well as for the net flux. The best results are obtained at Bering Strait, while the worst agreement is found at Davis Strait. However ORAS5 generally seems to overestimate the volume fluxes at all four straits. The uncertainty estimates in table 6 have to be used with caution, as they are only derived from the standard derivation and hence merely provide information about the monthly variability. The net fluxes of ArcGate and ORAS5 seem to be in relative

Strait	**ArcGate**	**ORAS5**	**RMSE_norm**
Net	0.14 ± 0.04	0.14 ± 0.10	0.62
Bering	-1.02 ± 0.49	-1.25 ± 0.49	0.31
BSO	-2.55 ± 1.04	-3.60 ± 1.13	0.52
Fram	1.71 ± 1.09	1.79 ± 1.05	0.57
Davis	2.00 ± 0.89	3.20 ± 0.71	0.79

Table 6: Mean values and calculated RMSEs of the individual volume fluxes and the net volume flux from ArcGate and Oras5. Units are Sverdrup (=10^6m3/s).

good agreement as the spatial and temporal mean over the considered period is equal

for both time series with a value of about 140 mSv, or 4400-4500 km3/yr. However the normalized RMSE indicates quite big differences between ArcGate and ORAS5, resulting from differences in the seasonal cycles.

To investigate this further figure 37 shows a comparison of merely the net fluxes (=freshwater fluxes) from ArcGate (blue) and ORAS5 (orange). Both time series future clear seasonalities and the position of maxima and minima is quite similar for both series, with the lowest values in winter month and the highest ones during summer. However there is a big difference concerning the height of the peaks itself with ORAS5 strongly overestimating both the maxima and the minima.

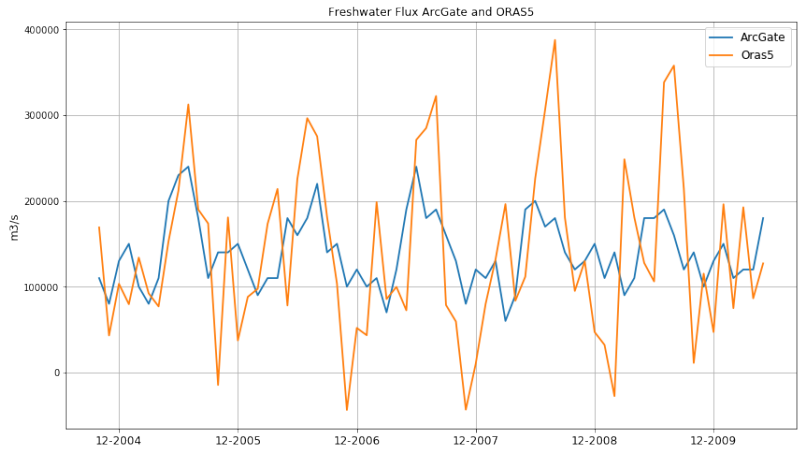

Figure 37: Freshwater fluxes from ArcGate and ORAS5.

Looking at equation 11 and assuming stationary conditions, the left side of the equation may be dropped. Subsequently freshwater flux should be equal to net precipitation over the ocean plus runoff from the Arctic Lands. Figure 38 shows the comparison between the direct fluxes from ArcGate and ORAS5 and the indirect calculated freshwater fluxes from ERA5 as well as from ERA-Interim. ERA-Interim, the precursor of ERA5, is considered as ORAS5 uses ERA-Interim as atmospheric forcing. The indirect calculated freshwater flux from ERA5 is very similar to the observed flux from the ArcGate project, only featuring slightly broader spring and summer peaks. Therefore the difference between ERA5 and the reanalysed freshwater flux from ORAS5 is quite big. The indirectly calculated flux from ERA-Interim agrees better with the high spring and summer peaks in ORAS5, however the strong winter minima in Oras5, that partly even reach negative values and hence characterise a winter net flux into the Arctic Ocean, are not present in any of the other products.

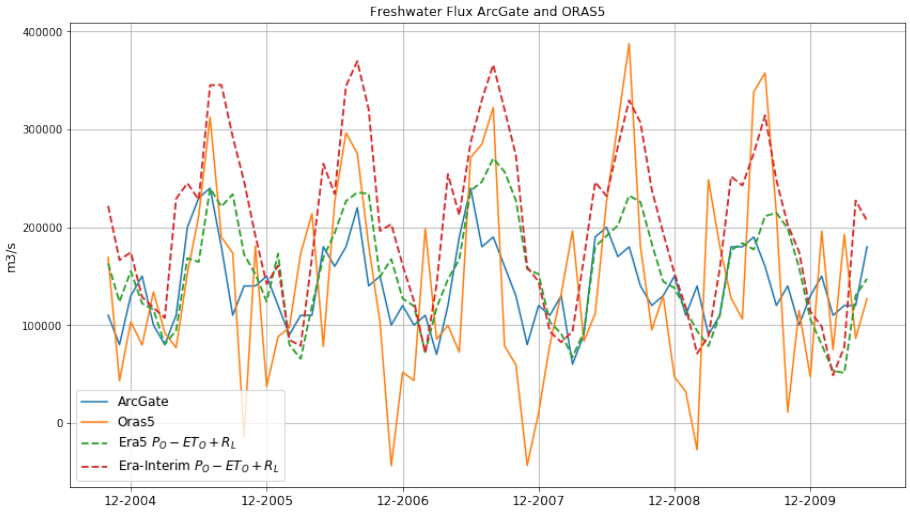

Figure 38: Comparison of net freshwater fluxes from ArcGate and ORAS5 with indirectly calculated fluxes from ERA5 and ERA-Interim.

5 Comparison with literature estimates

In order to compare the estimated fluxes with literature estimates, figure 5 is adapted with the values obtained in this study. Figure 39 shows the values obtained by Serreze et al. (2006) in black and values from this study in red. The oceanic and terrestrial domain viewed by Serreze et al. (2006) differs from the domain adapted here, as Serreze et al. (2006) set a boundary across the northern end of the CAA and hence they leave out Baffin Bay, the complicated channels of the CAA and the river catchments draining into it. Therefore the following comparison has to be viewed with caution and only serves to assess the magnitude of the various fluxes. For the atmospheric terms Serreze et al. (2006) use ERA-40 reanalysis and precipitation observations, calculate P-ET via the aerological method and get ET subsequently as residual of P-ET and P. For river discharge they combine observations with estimated contributions for the unmonitored regions and the oceanic fluxes are adopted from previous studies.

5.1 Budget Closure

With the data collected an attempt can be made to close the budget equations for atmosphere (eq. 7), land (eq. 9) and ocean (eq. 11). The atmospheric fluxes are all derived from ERA5 reanalyses, the oceanic fluxes are taken from ArcGate and for runoff ERA5-Land is used as it comes closest to the observed values. All fluxes are

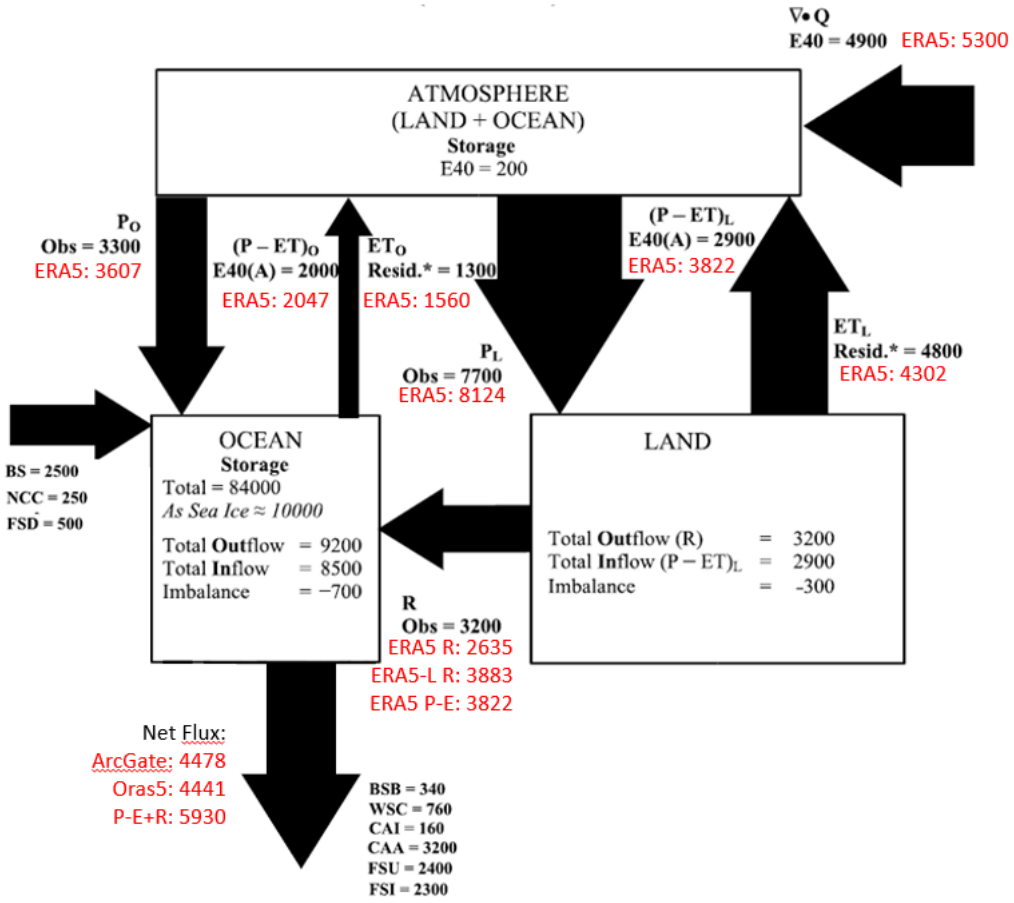

Figure 39: Figure from Serreze et al. (2006), adapted with values obtained in this study (red values). Units are km^3 per year for fluxes and km^3 for storage terms.

calculated as perennial means over their available period. That is 1979-2019 for ERA5, 1981-2019 for ERA5-Land and October 2004 to May 2010 for the oceanic fluxes from ArcGate.

Atmosphere:

$$\frac{\partial W}{\partial t} = (P_O + P_L) - (ET_O + ET_L) - \nabla \cdot \mathbf{Q} = 569 \ km^3/yr \tag{12}$$

Inserting all values into the equation, yields an imbalance of 569 km^3/yr. Considering that merely data from ERA5 was used, the difference between net precipitation and atmospheric moisture flux divergence seems quite big. Although atmospheric moisture storage has slightly changed over the past decades (see figure 16), it does not account for this much of a difference. Taken from figure 16, a change of roughly 0.7 kg/m^2 occurred

in the past 40 years, integrated over the whole Arctic area that is equal to a change of merely about 0.5 km^3 per year. Hence the difference between net precipitation and the moisture flux divergence has to have other causes. To some extent the errors may come from the biases that are typically present in surface variables from reanalysis. To investigate this further reliable observations of P and ET would be needed, however those are rather sparse in the Arctic area and not available for this study.

Land:

$$\frac{\partial M_L}{\partial t} = P_L - ET_L - R = -61\ km^3/yr \tag{13}$$

The terrestrial branch features a surprisingly small imbalance of -61 km^3/yr. This imbalance may be partly caused by the usage of ERA5-Land runoff, as ERA5-Land tends to slightly overestimate observed runoff (see section 4.3.1 and table 4). Furthermore the left side of the equation again is not equal to zero, as according to ERA5 and ERA5-Land soil moisture features a slight downward trend over the past decades (see figure 34).

Ocean:

$$\frac{\partial M_O}{\partial t} = P_O - ET_O + R - \nabla \cdot \mathbf{F} = 1452\ km^3/yr \tag{14}$$

Using P and ET from ERA5, R from ERA5-Land and F from ArcGATE observations, the imbalance for the Arctic OCean is rather big with 1452 km^3/yr. This imbalance is, at least to some extent, caused through an underestimation of the oceanic freshwater fluxes, as ice transports through the gateways are not specifically considered. Examining ArcGate freshwater fluxes in summer 2005, Tsubouchi et al.(2012) find a liquid freshwater export of 4636 km^3/yr whereto they add an extra 1261 km^3/yr accounting for Fram Strait sea ice export. Adding their value for sea ice, the imbalance in equation 14 shrinks to 191 km^3/yr.

6 Conclusion

The past sections gave a general overview of the Arctic freshwater branches and the processes amongst them and the individual parameters were assessed on trends and variabilities. This last chapter summarises the key results found in section 4.

Analysis of the atmospheric freshwater components revealed no significant trends averaged over the whole Arctic domain. However looking at the spatial distribution, some regions very well showed changes over the past 40 years. The central Arctic exhibited slight increases in ERA5 net precipitation, resulting mainly from negative evaporation trends. In contrast at Barents Sea, Kara Sea and the Beaufort Sea relatively strong increases in evaporation exceed slight precipitation increases, resulting in a decline of net precipitation. Hence those regions exhibit a decrease in freshwater delivery from the atmosphere to the surface.

The difference between P-ET and the divergence of moisture flux reaches a relative difference of up to 10% over the whole Arctic area. This difference may, at least to some extent, be caused by the biases present in surface variables from reanalysis, as the quantities P and ET are merely based on short-term forecasts,while the moisture flux convergence is a true analysis quantity that i.a. incorporates assimilation of air moisture and wind observations. The smaller the difference between net precipitation and moisture flux divergence, the closer the reanalysis comes to a hydrological balance, meaning that data assimilation has no net effect in influencing the divergence of moisture flux (Jakobson and Vihma, 2010).

Furthermore total precipitation over the Arctic was assessed on interannual variabilities and a strong correlation of 0.64 (0.70) could be found between NAO (AO) and Arctic precipitation north of 65°N.

The biggest discrepancies occurred for the hydrological land component runoff. Direct runoff from ERA5 showed strong negative trends and deviated greatly from observed runoff, while indirectly calculated runoff (P-ET) from ERA5 and direct runoff from ERA5-Land represented the actual runoff values quite good. The large difference between ERA5 and ERA5-Land runoff, reaching more than 20% summed over all 64 catchments, is likely caused by the land data assimilation system removing snow and soil moisture in ERA5. A distinct discontinuity between snowmelt and snowfall around

2004 was traced back to the IMS snow product introduced to the assimilation system. As snow schemes in the HTESSEL are known to melt snow too slowly, the assimilation in combination with the IMS snow cover data could remove excess snow in observation-sparse areas that was not melted by the model and hence produce those negative shifts in snowmelt. (Zsoter et al., 2020) However differences between snowmelt and snowfall are also present before 2004, indicating that assimilation likely contributed to negative snowmelt trends already before the IMS introduction. Additionally the higher resolution and lapse-rate correction in ERA5-Land could cause discrepancies. (Zsoter et al., 2020) The extremely low runoff values featured by GloFAS 2.1 could not be explained in the course of this study and would need further examination. As the values are even lower than ERA5 runoff, there's probably a problem in the hydrological LISFLOOD system or in the coupling between ERA5 runoff and LISFLOOD.

The oceanic branch was hard to assess, as data from ArcGate was only available for a very short period of time. Nevertheless for the period available fluxes from ArcGate, that are based mainly on observations, and indirectly calculated fluxes from ERA5 reanalysis show a similar progress.

Literatur

Aagaard, K. and E. C. Carmack (1989), The role of sea ice and other fresh waters in the Arctic circulation, *J. Geophys. Res.*, 94, 14, 485–14, 498. https://doi.org/10.1029/JC094iC10p14485.

Allen, M. and W. Ingram (2002), Constraints on Future Changes in Climate and the Hydrologic Cycle, *Nature*, 419, 224-32. https://doi.org/10.1038/nature01092.

Andresen, C., D. Lawrence, C. Wilson, A. McGuire, C. Koven, K. Schaefer, E. Jafarov, S. Peng, X. Chen, I. Gouttevin, E. Burke, S. Chadburn, D. Ji, D. Hayes and W. Zhang (2019), Soil Moisture and Hydrology Projections of the Permafrost Region: A Model Intercomparison, *The Cryosphere Discussions*, 1-20. https://doi.org/10.5194/tc-2019-144.

Arcitc Centre (n.d.*a*), Basic information about the Arctic. https://www.arcticcentre.org/EN/arcticregion, Accessed on 23.04.2020 13:05.

Arcitc Centre (n.d.*b*), Definitions of the Arctic region. https://www.arcticcentre.org/EN/arcticregion/Maps/definitions, Accessed on 23.04.2020 16:16.

AWI (2019), Maximizing the potential of Arctic Ocean Gateway array. https://www.awi.de/en/science/climate-sciences/physical-oceanography/projects/arcgate.html, Accessed on 28.06.2020 8:30.

Azetsu-Scott, K., B. Petrie, P. Yeats and C. Lee (2012), Composition and fluxes of freshwater through Davis Strait using multiple chemical tracers, *J. Geophys. Res.*, 117, C12011. https://doi.org/10.1029/2012JC008172.

Bacon, S., Y. Aksenov, S. Fawcett and G. Madec (2015), Arctic mass, freshwater and heat fluxes: Methods and modelled seasonal variability, *Philosophical transactions of the Royal Society*, Series A, Mathematical, physical, and engineering sciences, 373. http://doi.org/10.1098/rsta.2014.0169.

Balsamo G., A. Beljaars, K. Scipal, P. Viterbo, B. van den Hurk, M. Hirschi and A. K. Betts (2008), A Revised Hydrology for the ECMWF Model: Verification from Field Site to Terrestrial Water Storage and Impact in the Integrated Forecast System, *J. Hydrometeor.*, 10, 623–643. http://doi.org/10.1175/2008JHM1068.1.

Bintanja R. and F. M. Selten (2014), Future increases in Arctic precipitation linked to local evaporation and sea-ice retreat, *Nature*, 22, 509(7501):479-82. https://doi.org/10.1038/nature13259.

Bintanja, R., K. Van der Wiel, E. Van der Linden, J. Reusen, L. Bogerd, F. Krikken and F. Selten (2020), Strong future increases in Arctic precipitation variability linked to poleward moisture transport, *Science Advances*, 6. https://doi.org/10.1126/sciadv.aax6869.

Boisvert, L. N. and J. C. Stroeve (2015), The Arctic is becoming warmer and wetter as revealed by the Atmospheric Infrared Sounder, *Geophys. Res. Lett.*, 42, 4439– 4446. https://doi.org/10.1002/2015GL063775.

Box, J. E., W. T. Colgan, T. R. Christensen, N. M. Schmidt, M. Lund, F. W. Parmentier, ... M. S. Olsen (2019), Key indicators of Arctic climate change: 1971–2017, *Environ. Res. Lett.*, 14, 045010. https://doi.org/10.1088/1748-9326/aafc1b.

Cassano, J. J., P. Uotila, A. H. Lynch and E. N. Cassano (2007), Predicted changes in synoptic forcing of net precipitation in large Arctic river basins during the 21st century, *J. Geophys. Res.*, 112, G04S49. https://doi.org/10.1029/2006JG000332.

CDS (2019), ERA5 monthly averaged data on single levels from 1979 to present. https://doi.org/10.24381/cds.f17050d7.

Condron, A., P. Winsor, C. Hill and D. Menemenlis (2009), Simulated Response of the Arctic Freshwater Budget to Extreme NAO Wind Forcing, *J. Climate*, 22, 2422–2437. https://doi.org/10.1175/2008JCLI2626.1.

Cuny, J., P. Rhines and R. Kwok (2004), Davis Strait volume, freshwater and heat fluxes, *Deep Sea Research Part I: Oceanographic Research Papers*, 52, 519-542. https://doi.org/10.1016/j.dsr.2004.10.006.

Curry, B., C. Lee and B. Petrie (2010), Volume, Freshwater, and Heat Fluxes through Davis Strait, 2004-05, *Journal of Physical Oceanography*, 41, 429-436. https://doi.org/10.1175/2010JPO4536.1.

Davidson N.C. (2016), Yenisei River Basin and Lake Baikal (Russia). In: Finlayson C., Milton G., Prentice R., Davidson N. (eds) *The Wetland Book*. Springer, Dordrecht. https://doi.org/10.1007/978-94-007-6173-5_276-1.

Dee, D. P., P. Berrisford, P. Poli, R. Brugge, M. Fielding, M. Fuentes, P. W. Kållberg, S. Kobayashi, S. Uppala and A. Simmons (2011), The ERA-Interim archive Version 2.0, *ERA Report Series*, 1-23.

Degtyarev V. (2016), Lena River Basin (Russia). In: Finlayson C., Milton G., Prentice R., Davidson N. (eds) *The Wetland Book*. Springer, Dordrecht. https://doi.org/10.1007/978-94-007-6173-5_96-2

Déry, S. J. and E. F. Wood (2005), Decreasing river discharge in northern Canada, *Geophys. Res. Lett.*, 32, L10401. https://doi.org/10.1029/2005GL022845.

Dickson, R. R., T. J. Osborn, J. W. Hurrell, J. Meincke, J. Blindheim, B. Adlandsvik, T. Vinje, G. Alekseev and W. Maslowski (2000) The Arctic Ocean Response to the North Atlantic Oscillation, *J. Climate*, 13, 2671–2696. https://doi.org/10.1175/1520-0442(2000)013¡2671:TAORTT¿2.0.CO;2.

Dickson, R., B. Rudels, S. Dye, M. Karcher, J. Meincke and I. Yashayaev (2007), Current estimates of freshwater flux through Arctic and subarctic seas, *Progress In Oceanography*, 210-230. https://doi.org/10.1016/j.pocean.2006.12.003.

Dutra, E., P. Viterbo, P. M. A. Miranda and G. Balsamo (2012), Complexity of Snow Schemes in a Climate Model and Its Impact on Surface Energy and Hydrology, *J. Hydrometeor.*, 13, 521–538. https://doi.org/10.1175/JHM-D-11-072.1.

ECMWF (2020*a*), ERA5: data documentation. https://confluence.ecmwf.int/display/CKB/ERA5, Accessed on 21.06.2020 7:58.

ECMWF (2020*b*), ERA5-Land: data documentation. https://confluence.ecmwf.int/display/CKB/ERA5-Land, Accessed on 22.06.2020 16:05.

Foster, J., D. Robinson, D. Hall and T. Estilow (2008), Spring snow melt timing and changes over Arctic lands, *Polar Geography*, 31, 145-157. https://doi.org/10.1080/10889370802580185.

Frontier Scientists (2015), Discerning ocean currents at current. https://frontierscientists.com/2015/06/discerning-ocean-currents-current/, Accessed on 13.06.2020 07:50.

Groves, D. G. and J. A. Francis (2002), Variability of the Arctic atmospheric moisture budget from TOVS satellite data, *J. Geophys. Res.*, 107(D24), 4785. https://doi.org/10.1029/2002JD002285.

Hakkinen, S. and A. Proshutinsky (2004), Freshwater content variability in the Arctic Ocean, *J. Geophys. Res.*, 109, C03051. https://doi.org/10.1029/2003JC001940.

Hantel, M. and L. Haimberger (2016), *Grundkurs Klima*, vol. 1. Springer Spektrum, ISBN:978-3-662- 48192-9. https://doi.org/10.1007/978-3-662-48193-6.

Harrigan, S., E. Zsótér, L. Alfieri, C. Prudhomme, P. Salamon, F. Wetterhall, ... F. Pappenberger (2020), GloFAS-ERA5 operational global river discharge reanalysis 1979–present. https://doi.org/10.5194/essd-2019-232.

Hersbach, H., B. Bell, P. Berrisford, S. Hirahara, A. Horányi, J. Muñoz Sabater, ... J.-N. Thépaut (2020), The ERA5 Global Reanalysis, *Quarterly Journal of Royal Meteorological Society*, 146. https://doi.org/10.1002/qj.3803.

Holland, M. M., J. Finnis and M. C. Serreze (2006), Simulated Arctic Ocean Freshwater Budgets in the Twentieth and Twenty-First Centuries, *J. Climate*, 19, 6221–6242. https://doi.org/10.1175/JCLI3967.1.

Holmes, R. M., M. T. Coe, G.J. Fiske, T. Gurtovaya, J. W. McClelland, A. I. Shiklomanov, R. G. M. Spencer, S. E. Tank and A. V. Zhulidov (2013), Climate change impacts on the hydrology and biogeochemistry of Arctic Rivers, In: Global Impacts of Climate Change on Inland Waters (eds C.R. Goldman, M. Kumagai and R.D. Robarts). https://doi.org/10.1002/9781118470596.ch1.

Holmes, R. M., A. I. Shiklomanov, A. Suslova, M. Tretiakov, J. W. McClelland, R. G. M. Spencer and S. E. Tank (2018), River Discharge, Arctic Report Card: Update for 2018. https://arctic.noaa.gov/Report-Card/Report-Card-2018/ArtMID/7878/ArticleID/786/River-Discharge.

A. R. Hurley (2014), Comparison and validation of Arctic precipitation fields from three atmospheric reanalyses: CFSR, MERRA, ERA-Interim, *University of Colorado*

IPCC (2013), Climate Change 2013: The Physical Science Basis. Contribution of Working Group I to the Fifth Assessment Report of the Intergovernmental Panel on Climate Change [Stocker, T.F., D. Qin, G.-K. Plattner, M. Tignor, S.K. Allen, J. Boschung, A. Nauels,

Y. Xia, V. Bex and P.M. Midgley (eds.)], *Cambridge University Press*, Cambridge, United Kingdom and New York, NY, USA, 1535 pp.

Jakobson, E. and T. Vihma (2010), Atmospheric moisture budget in the Arctic based on the ERA-40 reanalysis, *Int. J. Climatol.*, 30: 2175-2194. https://doi.org/10.1002/joc.2039.

Jakobsson, M. (2002), Hypsometry and volume of the Arctic Ocean and its constituent seas, *Geochem. Geophys. Geosyst.*, 3(5), 1028. https://doi.org/10.1029/2001GC000302.

Lammers, R. B., A. I. Shiklomanov, C. J. Vörösmarty, B. M. Fekete and B. J. Peterson (2001), Assessment of contemporary Arctic river runoff based on observational discharge records, *J. Geophys. Res.*, 106, 3321– 3334. https://doi.org/10.1029/2000JD900444.

Lewis, E., E. Jones, P. Lemke, T. Prowse, and P. Wadhams (2000), The Freshwater Budget of the Arctic Ocean, *NATO Science Series*. https://doi.org/10.1007/978-94-011-4132-1.

Mayer, M., L. Haimberger, M. Pietschnig and A. Storto (2016), Facets of Arctic energy accumulation based on observations and reanalyses 2000–2015, *Geophys. Res. Lett.*, 43, 10,420– 10,429. https://doi.org/10.1002/2016GL070557.

Mayer, M., S. Tietsche, L. Haimberger, T. Tsubouchi, J. Mayer and H. Zuo (2019), An Improved Estimate of the Coupled Arctic Energy Budget, *J. Climate*, 32, 7915–7934. https://doi.org/10.1175/JCLI-D-19-0233.1.

Madec, G., and M. Imbard (1996), A global ocean mesh to overcome the north pole singularity, *Clim. Dyn.*, 12, 381-388.

McClelland, J. W., R. M. Holmes, B. J. Peterson and M. Stieglitz (2004), Increasing river discharge in the Eurasian Arctic: Consideration of dams, permafrost thaw, and fires as potential agents of change, *J. Geophys. Res.*, 109, D18102. https://doi.org/10.1029/2004JD004583.

J. Muñoz-Sabater (2017), ERA5-Land: A new state-of-the-art Global Land Surface Reanalysis Dataset, *31st Conference on Hydrology - 2017 AMS annual meeting*, Seattle, US.

NASA (2002), Davis Strait. https://visibleearth.nasa.gov/images/57989/davis-strait, Accessed on 09.06.2020 08:30.

NASA (2020), Arctic Sea Ice Minimum. https://climate.nasa.gov/vital-signs/arctic-sea-ice/, Accessed on 10.09.2020 07:20.

NEMO (2017), ORCA family: global ocean with tripolar grid. https://www.nemo-ocean.eu/doc/node108.html, Accessed on 08.06.2020 12:30.

Peterson, B. J., R. M. Holmes, J. W. McClelland, C. J. Vörösmarty, R. B. Lammers, I. A. Shiklomanov and S. Rahmstorf (2002), Increasing river discharge to the Arctic Ocean, *Science*, 298, 2171– 2173. https://doi.org/10.1126/science.1077445.

Pietschnig, M., M. Mayer, T. Tsubouchi, A. Storto, S. Stichelberger and Leopold Haimberger (2018), Volume transports and temperature distributions in the main Arctic Gateways: A comparative study between an ocean reanalysis and mooring-derived data, *eartharxiv*, https://doi.org/10.31223/osf.io/5hg3z

Rabe, B. , P. Dodd, E. Hansen, E. Falck, U. Schauer, A. Mackensen, A. Beszczynska-Möller, G. Kattner, E. Rohling and K. Cox (2013), Liquid export of Arctic freshwater components through the Fram Strait 1998 – 2011, *Ocean Science*, 9, pp. 91-109. https://doi.org/10.5194/os-9-91-2013.

Rapaić, M., R. Brown, M. Markovic and D. Chaumont (2015), An Evaluation of Temperature and Precipitation Surface-Based and Reanalysis Datasets for the Canadian Arctic, 1950–2010, *Atmosphere-Ocean*, 53:3, 283-303. https://doi.org/10.1080/07055900.2015.1045825

Rawlins, M. A., M. Steele, M. M. Holland, J. C. Adam, J. E. Cherry, J. A. Francis, ... T. Zhang (2010), Analysis of the Arctic System for Freshwater Cycle Intensification: Observations and Expectations, *J. Climate*, 23, 5715–5737. https://doi.org/10.1175/2010JCLI3421.1.

Robinson J. L. (2019), Mackenzie River, *Encyclopaedia Britannica*. https://www.britannica.com/place/Mackenzie-River, Accessed on 21.09.2020 18:50.

Rogers, A. N., D. H. Bromwich, E. N. Sinclair and R. I. Cullather (2001), The atmospheric hydrologic cycle over the Arctic Basin from re-analyses. Part II: Interannual variability, *J. Clim.*, 14, 2414– 2429. https://doi.org/10.1175/1520-0442(2001)014¡2414:TAHCOT¿2.0.CO;2.

Semmens, K., J. Ramage, A. Bartsch and G. Liston (2013), Early snowmelt events: Detection, distribution, and significance in a major sub-arctic watershed, *Environmental Research Letters*, 8. https://doi.org/10.1088/1748-9326/8/1/014020.

Serreze, M. C., R. G. Barry and J. E. Walsh (1995), Atmospheric Water Vapor Characteristics at 70°N, *J. Climate*, 8, 719–731. https://doi.org/10.1175/1520-0442(1995)008¡0719:AWVCA¿2.0.CO;2.

Serreze, M. C., F. Carse, R. G. Barry and J. Rogers (1997), Icelandic Low Cyclone Activity: Climatological Features, Linkages with the NAO, and Relationships with Recent Changes in the Northern Hemisphere Circulation, *Journal of Climate*, 10, 453–464 10. https://doi.org/10.1175/1520-0442(1997)010¡0453:ILCACF¿2.0.CO;2.

Serreze, M. C., J. E. Walsh, F. S. Chapin, T. Osterkamp, M. Dyurgerov, V. Romanovsky, W. C. Oechel, J. Morison, T. Zhang and R. G. Barry (2000), Observational Evidence of Recent Change in the Northern High-Latitude Environment, *Climatic Change* 46, 159–207. https://doi.org/10.1023/A:1005504031923.

Serreze, M. C., D. H. Bromwich, M. P. Clark, A. J. Ertringer, T. Zhang, T. R. Lammers (2002), Large-scale hydro-climatology of the terrestrial Arctic drainage system, *J. Geophys. Res.*, 107, 8160. https://doi.org/10.1029/2001JD000919.

Serreze, M. C., A. P. Barrett, A. G. Slater, R. A. Woodgate, K. Aagaard, R. B. Lammers, M. Steele, R. Moritz, M. Meredith and C. M. Lee (2006), The large-scale freshwater cycle of the Arctic, *J. Geophys. Res.*, 111, C11010. https://doi.org/10.1029/2005JC003424.

Serreze, M. C., and R. G. Barry (2014), *The Arctic Climate System* (Second edi). Cambridge: Cambridge University Press. https://doi.org/10.1017/CBO9781139583817.

Sheffield, J. and E. Wood (2008), Global Trends and Variability in Soil Moisture and Drought Characteristics, 1950 2000, from Observation-Driven Simulations of the Terrestrial Hydrologic Cycle, *Journal of Climate*, 21. https://doi.org/10.1175/2007JCLI1822.1.

Shiklomanov, A.I., R.M. Holmes, J.W. McClelland, S.E. Tank and R.G.M. Spencer (2020), Arctic Great Rivers Observatory, Discharge Dataset, Version YYYYMMDD. https://www.arcticrivers.org/data.

Smedsrud, L. H., I. Esau, R. B. Ingvaldsen, T. Eldevik, P. M. Haugan, C. Li, ... S. A. Sorokina (2013), The role of the Barents Sea in the Arctic climate system, *Reviews of Geophysics*, 51(3), 415–449. https://doi.org/10.1002/rog.20017.

Steele, M. and W. Ermold (2004), Salinity trends on the Siberian shelves, *Geophys. Res. Lett.*, 31, L24308. https://doi.org/10.1029/2004GL021302.

Steele, M. and W. Ermold (2007), Steric Sea Level Change in the Northern Seas, *Journal of Climate*, 20. https://doi.org/10.1175/JCLI4022.1.

Streletskiy, D., O. Anisimov and A. Vasiliev (2015), Chapter 10 - Permafrost Degradation. In: Shroder, J.F., W. Haeberli and C. Whiteman (Eds.), Snow and Ice-Related Hazards, Risks and Disasters, *Academic Press: Boston*, pp. 303-344. https://doi.org/10.1016/B978-0-12-394849-6.00010-X.

Swift, J. H., K. Aagaard, L. Timokhov and E. G. Nikiforov (2004), Long-term variability of Arctic Ocean waters: Evidence from a reanalysis of the EWG data set, *J. Geophys. Res.*, 110. https://doi.org/10.1029/2004JC002312.

The Arctic Sytsem (n.d.), The sea and ocean currents. http://www.arcticsystem.no/en/outsideworld/oceancurrents, Accessed on 15.06.2020 8:09.

Tsubouchi, T., S. Bacon, A. C. Naveira Garabato, Y. Aksenov, S. W. Laxon, E. Fahrbach, A. Beszczynska-Möller, E. Hansen, C. M. Lee and R. B. Ingvaldsen (2012), The Arctic Ocean in summer: A quasi-synoptic inverse estimate of boundary fluxes and water mass transformation, *J. Geophys. Res.*, 117, C01024. https://doi.org/10.1029/2011JC007174.

Tsubouchi, T., and Coauthors (2018), The Arctic Ocean Seasonal Cycles of Heat and Freshwater Fluxes: Observation-Based Inverse Estimates, *J. Phys. Oceanogr.*, 48, 2029–2055. https://doi.org/10.1175/JPO-D-17-0239.1.

Villamil-Otero, G. A., J. Zhang, J. X. He and X. Zhang (2018), Role of extratropical cyclones in the recently observed increase in poleward moisture transport into the Arctic Ocean, *Adv. Atmos. Sci.*, 35(1), 85–94. https://doi.org/10.1007/s00376-017-7116-0.

Walsh, J. E., V. Kattsov, D. Portis and V. Meleshko, (1998), Arctic Precipitation and Evaporation: Model Results and Observational Estimates, *J. Climate*, 11, 72–87. https://doi.org/10.1175/1520-0442(1998)011¡0072:APAEMR¿2.0.CO;2.

Wang, X. and J. R. Key (2005), Arctic surface, cloud, and radiation properties based on the AVHRR polar pathfinder dataset. Part II: Recent trends, *J. Climate*, 18, 2575– 2593. https://doi.org/10.1175/JCLI3439.1.

Wang, C., R. Graham, K. Wang, S. Gerland and M. Granskog (2019), Comparison of ERA5 and ERA-Interim near surface air temperature, snowfall and precipitation over Arctic

sea ice: Effects on sea ice thermodynamics and evolution, *The Cryosphere*, 13, 1661-1679. https://doi.org/10.5194/tc-13-1661-2019.

White, D., L. Hinzman, L. Alessa, J. Cassano, M. Chambers, K. Falkner, ... T. Zhang (2007), The arctic freshwater system: Changes and impacts, *J. Geophys. Res.*, 112, G04S54, https://doi.org/10.1029/2006JG000353.

Woodgate, R. A. and K. Aagaard (2005), Revising the Bering Strait freshwater flux into the Arctic Ocean, *Geophys. Res. Lett.*, 32, L02602. https://doi.org/10.1029/2004GL021747.

Woodgate, R. A., K. Aagaard and T. J. Weingartner (2006), Interannual changes in the Bering Strait fluxes of volume, heat and freshwater between 1991 and 2004, *Geophys. Res. Lett.*, 33, L15609. https://doi.org/10.1029/2006GL026931.

Woodgate, R. A., T. J. Weingartner and R. Lindsay (2012), Observed increases in Bering Strait oceanic fluxes from the Pacific to the Arctic from 2001 to 2011 and their impacts on the Arctic Ocean water column, *Geophys. Res. Lett.*, 39, L24603. https://doi.org/10.1029/2012GL054092.

Xie, P. and P. A. Arkin (1996), Analyses of global monthly precipitation using gauge observations, satellite estimates and numerical model prediction, *J. Climate*, 9, 840–858. https://doi.org/10.1175/1520-0442(1996)009¡0840:AOGMPU¿2.0.CO;2.

Yang, D., D. Kane, L. Hinzman, X. Zhang, T. Zhang and H. Ye (2002), Siberian Lena River hydrologic regime and recent change, *J. Geophys. Res.*, 107(D23), 4694. https://doi.org/10.1029/2002JD002542.

Yang, D., D. Robinson, Y. Zhao, T. Estilow and B. Ye (2003), Streamflow response to seasonal snow cover extent changes in large Siberian watersheds, *J. Geophys. Res.*, 108(D18), 4578. https://doi.org/10.1029/2002JD003149.

Yang, D., B. Ye and A. Shiklomanov (2004*a*), Discharge Characteristics and Changes over the Ob River Watershed in Siberia, *J. Hydrometeor.*, 5, 595– 610. https://doi.org/10.1175/1525-7541(2004)005¡0595:DCACOT¿2.0.CO;2.

Yang, D., B. Ye and D. Kane (2004*b*), Streamflow changes over Siberian Yenisei River Basin, *Journal of Hydrology*, 296, 59-80. https://doi.org/10.1016/j.jhydrol.2004.03.017.

Yang, D., Y. Zhao, R. Armstrong, D. Robinson and M. J. Brodzik (2007), Streamflow response to seasonal snow cover mass changes over large Siberian watersheds, *J. Geophys. Res.*, 112, F02S22. https://doi.org/10.1029/2006JF000518.

Ye, B., D. Yang and D. Kane (2003), Changes in Lena River streamflow: Human impacts versus natural variations, *Water Resour. Res.*, 39(7), 1200. https://doi.org/10.1029/2003WR001991.

Zhang, X., J. He, J. Zhang, I. Polyakov, R. Gerdes, J. Inoue and P. Wu (2012), Enhanced poleward moisture transport and amplified northern high-latitude wetting trend, *Nature Clim Change* 3, 47–51. https://doi.org/10.1038/nclimate1631.

Zsótér, E., H. Cloke, E. Stephens, P. de Rosnay, J. Muñoz-Sabater, C. Prudhomme and F. Pappenberger (2019), How Well Do Operational Numerical Weather Prediction Configurations Represent Hydrology?, *J. Hydrometeor.*, 20, 1533–1552. https://doi.org/10.1175/JHM-D-18-0086.1.

Zsótér, E, H. Cloke, C. Prudhomme, S. Harrigan, P. de Rosnay, P, J. Muñoz-Sabater and E. Stephens (2020), Trends in the GloFAS-ERA5 river discharge reanalysis, *ECMWF TechnicalMemoranda* 871. https://doi.org/10.21957/p9jrh0xp.

Zuo, H., M. Alonso-Balmaseda, K. Mogensen and S. Tietsche (2018), OCEAN5: The ECMWF Ocean Reanalysis System and its Real-Time analysis component, *ECMWF Technical-Memoranda* 823. https://doi.org/10.21957/la2v0442.

List of Tables

List of Figures